

Review

Open Access



Recent research progress in the application of $\text{Na}_3\text{V}_2(\text{PO}_4)_2\text{F}_3$ cathode materials in sodium-ion batteries: synthesis, modification, and battery optimization

Yining Liang^{1,2}, Lin Xu¹, Zhengjian Chen^{1,2}, De Ning¹, Zhipeng Sun²

¹Zhuhai Institute of Advanced Technology, Shenzhen Institutes of Advanced Technology, Chinese Academy of Sciences, Zhuhai 519000, Guangdong, China.

²School of Materials and Energy, Guangdong University of Technology, Guangzhou 510006, Guangdong, China.

Correspondence to: Prof. Zhengjian Chen, Zhuhai Institute of Advanced Technology, Shenzhen Institutes of Advanced Technology, Chinese Academy of Sciences, Hagongda Road, No.2, Zhuhai 519000, Guangdong, China; School of Materials and Energy, Guangdong University of Technology, Waihuan Xi Road, No.100, Guangzhou 510006, Guangdong, China. E-mail: chenzhengjian@ziat.ac.cn; Dr. De Ning, Zhuhai Institute of Advanced Technology, Shenzhen Institutes of Advanced Technology, Chinese Academy of Sciences, Hagongda Road, No.2, Zhuhai 519000, Guangdong, China. E-mail: de.ning@siat.ac.cn; Prof. Zhipeng Sun, School of Materials and Energy, Guangdong University of Technology, Waihuan Xi Road, No.100, Guangzhou 510006, Guangdong, China. E-mail: zpsunxj@gdut.edu.cn

How to cite this article: Liang, Y.; Xu, L.; Chen, Z.; Ning, D.; Sun, Z. Recent research progress in the application of $\text{Na}_3\text{V}_2(\text{PO}_4)_2\text{F}_3$ cathode materials in sodium-ion batteries: synthesis, modification, and battery optimization. *Energy Mater.* **2025**, *5*, 500115. <https://dx.doi.org/10.20517/energymater.2024.306>

Received: 29 Dec 2024 **First Decision:** 25 Feb 2025 **Revised:** 23 Apr 2025 **Accepted:** 14 May 2025 **Published:** 6 Jun 2025

Academic Editor: Wei Tang **Copy Editor:** Shu-Yuan Duan **Production Editor:** Shu-Yuan Duan

Abstract

Sodium vanadium fluorophosphate [$\text{Na}_3\text{V}_2(\text{PO}_4)_2\text{F}_3$, NVPF], as a sodium (Na) super ionic conductor material, has attracted significant interest as a very promising cathode material for sodium-ion batteries due to its structural stability, rapid ion transport capability, and high operating potential. However, the insulating $[\text{PO}_4]$ units in NVPF isolate the V atoms, which results in low intrinsic electron conductivity and poor overall electrochemical performance, and the high cost also represents critical challenge that has impeded its widespread use. In recent years, the research focus has shifted to an enhancement of scalable fabrication technologies and improvement of operational robustness under extreme conditions. This has meant a realignment of the research paradigm from the modification of single materials to an adaptive design of the entire battery system. This review assesses the research conducted on NVPF cathodes over the past three years from several perspectives, focusing on the feasible application of materials over a wide temperature range at high voltages, summarizing the challenges and required development strategies in future research.



© The Author(s) 2025. **Open Access** This article is licensed under a Creative Commons Attribution 4.0 International License (<https://creativecommons.org/licenses/by/4.0/>), which permits unrestricted use, sharing, adaptation, distribution and reproduction in any medium or format, for any purpose, even commercially, as long as you give appropriate credit to the original author(s) and the source, provide a link to the Creative Commons license, and indicate if changes were made.



Keywords: Sodium-ion battery, sodium vanadium fluorophosphate, cathode materials synthesis, materials modification, battery optimization

INTRODUCTION

The negative environmental impact associated with the use of fossil fuels has driven the development of alternative renewable energy technologies, such as solar and wind power^[1], which has prompted significant research activity with respect to efficient electrochemical energy storage technologies for practical application^[2,3]. Lithium-ion batteries (LIBs) have emerged as viable options, exhibiting low self-discharge rates and high energy density^[4-6]. However, the widespread application of LIBs has been limited by the high cost and uneven distribution of lithium resources^[7-9]. In this context, sodium-ion batteries (SIBs) have been the subject of appreciable research as they are not subject to resource constraints, and can be operated safely at a low cost^[10-12]. As a homologous element, sodium possesses similar physicochemical properties to lithium, and some of the technologies and strategies established for LIBs can be applied to SIBs. Moreover, inexpensive aluminum foil can be used as the anode current collector in SIBs, reducing associated costs^[13,14]. However, SIBs exhibit low Na^+ transport rates, low energy density, and a limited reversible capacity^[15]. Therefore, it is necessary to improve SIB cycle stability and energy density in order to enable effective application, which requires significant scientific research and engineering technology advancements.

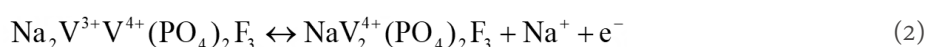
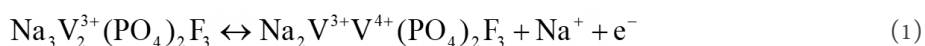
The electrochemical performance of SIBs is dependent on the inherent chemical properties of the electrode materials^[16-18]. Moreover, the cathode materials largely determine the device mass and output voltage^[19-23]. Currently, the SIB cathode materials can be divided into three categories: transition metal oxides^[24-28], Prussian blue analogs^[29-40], and polyanionic compounds (PACs)^[41-45]. Transition metal oxides exhibit a high specific capacity and facile synthesis, but the associated low average voltage, low energy density, poor cycle stability, and humidity sensitivity must be addressed^[46]. Prussian blue analogs have an open framework, abundant redox active sites, good structural stability, and large ion channels, but the coulombic efficiency and cycle stability are affected by lattice defects and crystal water^[47,48]. PACs are characterized by superior structural and thermal stability with enhanced ion diffusion dynamics that contribute to cycle stability and safety^[49,50]. In particular, $\text{Na}_3\text{V}_2(\text{PO}_4)_2\text{F}_3$ (NVPF) as a sodium (Na) super ionic conductor (NASICON), has been reported to deliver a high output voltage (3.95 V) and energy density (up to 500 Wh kg^{-1}) as a result of the highly ionic F-V bond, which enables an electrochemical output comparable to lithium iron phosphate-based LIBs^[51,52]. However, there are a number of challenges in terms of NVPF practical application, including the low intrinsic conductivity, high structural stress during electrochemical processes, and the high cost of vanadium^[53]. In order to improve electrochemical performance and reduce costs, it is necessary to adopt effective strategies for enhancing conductivity and Na^+ diffusion kinetics, and establish an effective commercially viable vanadium alternative.

Previous reviews predominantly focused on the intrinsic properties and singular modifications of NVPF^[53-55], primarily confined to laboratory-scale optimizations, while insufficient attention was paid to the extreme operational conditions and cost-effectiveness. This review constructs a multi-scale collaborative research framework “atom-interface-system”, breaking through the conventional singular emphasis on intrinsic material performance in the existing reviews. By incorporating high-entropy design, dynamic failure mechanisms, extreme-condition adaptability, and scalable manufacturing into a systematic analysis, we propose a reference technical roadmap to advance the industrial application of NVPF. The existing challenges in NVPF research are noted and future developments are outlined with the goal of realizing the practical application of high-performance NVPF systems.

CRYSTAL STRUCTURE AND PROPERTIES OF NVPF

Sodium vanadium fluorophosphate exhibits a typical NASICON structure, consisting of a three-dimensional (3D) framework formed by $[\text{V}_2\text{O}_8\text{F}_3]$ double octahedra and $[\text{PO}_4]$ tetrahedra linked through oxygen atoms. In this structure, the double octahedral units are connected by fluorine atoms, whereas the tetrahedral units are connected by oxygen atoms. The presence of $[\text{PO}_4]$ facilitates rapid migration of Na^+ within the framework and stabilizes the structure during metal redox processes.

Structural analysis of NVPF reveals minor orthorhombic lattice distortions localized on the (*h*00) and (0*k*0) crystallographic planes, with Rietveld refinement confirming the space group as *Amam*^[56]. The Na^+ ions occupy three distinct crystallographic sites (labeled Na1, Na2, and Na3) with refined occupancy ratios of 1:4/3:2/3, respectively [Figure 1A]. In a subsequent study, the desodiation process of $\text{Na}_3\text{V}_2(\text{PO}_4)_2\text{F}_3$ (Na_3VPF) was elucidated by *in situ* X-ray diffraction (XRD) analysis^[57]. As shown in Figure 1B, (Na_3VPF) (space group *Amam*) initially forms distinct intermediate phases during desodiation, including $\text{Na}_{2.4}\text{VPF}$, $\text{Na}_{2.2}\text{VPF}$ (*I4/mmm*), Na_2VPF (*I4/mmm*), and $\text{Na}_{1.8-1.3}\text{VPF}$ (*I4/mmm*), before ultimately transforming into NaVPF (*Cmc21*). In this process, the space group transitions sequentially from *Amam* to *I4/mmm* and finally to *Cmc21*. This structural evolution enables a two-electron transfer reaction, delivering a theoretical specific capacity of approximately 128 mAh g⁻¹. The structural evolution of NVPF and the sodium insertion/extraction processes are expressed in^[58]:



It should be noted that NVPF suffers from intrinsically poor electronic conductivity ($\sim 10^{-12}$ S cm⁻¹) due to the insulating $[\text{PO}_4]$ tetrahedra that spatially separate V atoms and impede electron transport. Moreover, repeated Na^+ insertion/extraction induces significant structural stress and anisotropic volume fluctuations, which serve to degrade mechanical stability and lead to a severe loss of capacity during cycling. The advantages and intrinsic challenges associated with NVPF are illustrated schematically in Figure 1C.

In the synthesis of NVPF, factors such as the carbon source selection and reaction conditions (temperature and pH) may result in fluorine loss. Fluorine deficiency disrupts the corner-sharing connectivity of $[\text{PO}_4]$ tetrahedra in the NASICON framework, destabilizing the 3D ion channels. This structural distortion triggers localized stress accumulation and significantly lowers the Na^+ migration rate^[59]. At a low fluorine content, irreversible phase transitions (such as the transition from high-pressure to low-pressure regions) occur during the charge/discharge process, accelerating structural collapse^[60]. Moreover, the corrosion acid (HF) induced by trace H_2O at the NVPF/Al collector interface further causes fluorine loss, degradation of crystal structure, increase in polarization voltage, and shedding of some active materials, leading to a rapid capacity decline^[61]. Fluorine loss can be effectively mitigated by optimizing the carbon source, process temperature, and anion regulation.

NVPF SYNTHESIS

A number of NVPF synthesis procedures have been reported, including solid-state^[62-66], sol-gel^[67-70], spray drying^[71-73], hydrothermal/solvothermal^[74-76], and electrostatic spinning^[77-79] methods. In addition, carbon coating, calcination, microwave treatment, and auxiliary reagents have been considered.

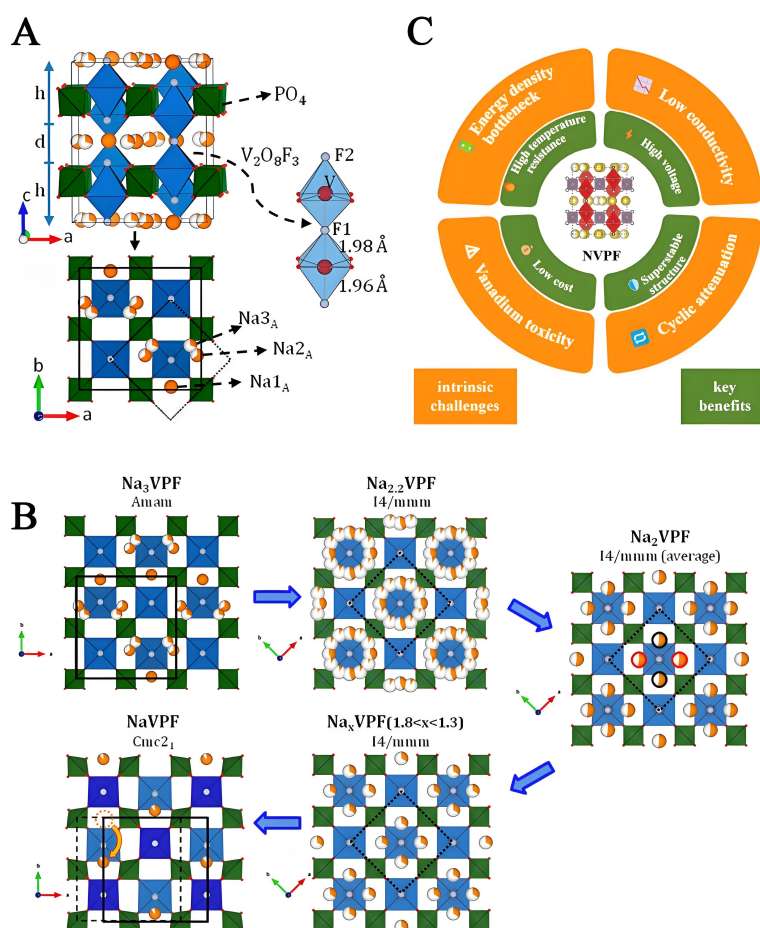


Figure 1. (A) Crystal structure of NVPF with the $Amam$ space group; (B) Corresponding crystal structural evolution of NVPF during Na^+ extraction. Reproduced with permission^[57]. Copyright 2015, American Chemical Society; (C) The key benefits and intrinsic challenges of NVPF cathodes in SIBs. NVPF: $\text{Na}_3\text{V}_2(\text{PO}_4)_2\text{F}_3$; SIB: sodium-ion battery.

Solid-state method

The solid-state procedure is easy to operate with a low associated cost, typically involving mechanical grinding and sintering^[80]. An increase in calcination temperature and the use of nanoscale raw materials can improve product purity and reduce overall reaction time.

Minart *et al.*^[81] reported dense and crystalline carbon-coated $\text{Na}_3\text{V}_2(\text{PO}_4)_2\text{F}_3$ (NVPF@C) nanoparticles resulting from solid-state synthesis, with a tap density of 1.4 g cm^{-3} (increased by 40%) following mechanical grinding, which represents the highest published value. The mechanical processing reduced the size of the particles and crystals while retaining the NVPF structure and surface chemical properties.

In the case of carbon thermal reduction (CTR), the carbon source is a critical consideration, serving as a reducing agent and coating layer to improve NVPF electronic conductivity. A number of organic carbon (glucose^[66] and bitumen^[64]) and inorganic carbon (acetylene black^[82] and super-phosphorus^[83]) sources have been considered. Different carbon sources were mixed with V_2O_5 and $\text{NH}_4\text{H}_2\text{PO}_4$ by ball-milling, and sintered at 800°C to prepare carbon-coated NVPF materials (C-NVPF)^[84]. Samples prepared using glucose as the sole carbon source delivered the best electrochemical performance in SIBs. Tannic acid has been employed as a chelating agent and carbon source to prepare a carbon-coated composite [NVPF composite

coated by tannic acid-derived carbon (NVPF@C-T)], using a combination of solid-state and sol-gel methods^[85]. By introducing tannic acid in two stages, a comprehensive and consistent carbon coating layer can be successfully created which significantly enhances the electronic conductivity of NVPF, facilitates the diffusion of Na⁺, and safeguards NVPF from corrosion caused by the electrolyte.

Citric acid was used as both a reducing agent and a carbon source in the synthesis of C-NVPF using surface ball-milling [Figure 2A]^[86]. The carbon coating improved conductivity and inhibited the aggregation of nanoparticles. The low voltage platform and decreased energy density due to the formation of NVP can be addressed by employing ball-milling to substitute Al for V in preparing NVAPF^[87]. The partial substitution of Al for V alters the local electronic states, enhancing the stability of F, where kinetic studies have confirmed an increase in Na⁺ migration rate.

Although the NVPF product generated by solid-state synthesis has a high phase purity, the electrochemical performance is affected by poor compositional homogeneity and a wide particle size distribution. It is necessary to further optimize the solid-state synthesis procedure in order to obtain NVPF with a uniform composition.

Hydrothermal/solvothermal method

Applying a hydrothermal/solvothermal synthesis enables materials synthesis to generate a product that effectively alleviates structural stress during electrochemical operation. For instance, a microwave-assisted hydrothermal procedure has been used to uniformly distribute NVPF on reduced graphene oxide (rGO), where NVPF nanocuboids coated with rGO (NVPF@rGO) were obtained after calcination^[88]. Al-Marri^[89] reported the synthesis of NVPF/rGO with a 3D conductive structure using a simple hydrothermal/solvent thermal reduction process. With the help of rGO, NVPF/rGO exhibited improved surface kinetics and diminished polarization, ultimately resulting in enhanced rate performance and extended cycle stability. The application of phosphomolybdic acid (PMA) as a crystal plane inducer served to increase adsorption and surface energy, accelerating the growth of NVPF crystals, and resulting in rectangular NVPF with continuous ionic diffusion paths. A nitrogen-doped carbon-coated rectangular NVPF cathode material (c-NVPF@NC) was synthesized by a PMA-assisted hydrothermal method [Figure 2B]^[90].

The grain size and vacancy defects can be effectively adjusted by varying the annealing temperature. For example, a NVPF electrode material obtained using hydrothermal method and subsequent thermal annealing at 350 °C exhibited a specific capacitance of 167.73 F g⁻¹ and a capacitance retention of 85%^[91]. Lin *et al.*^[92] studied the crystallization of NaH₂PO₄-VOSO₄-NaF-H₂O under hydrothermal conditions, where Na₃V₂O_{2x}(PO₄)₂F_{3-2x} was produced at 170 °C after 2 h with vanadium present in mixed valence states (V³⁺ and V⁴⁺). Varying the synthesis time, vanadium source, or the addition of reducing agents resulted in the formation of different NVPF pure phases. The unique pore structure of the NVPF cathode offers more active sites and promotes the diffusion of Na⁺. For example, tNVPF@C with a dense microsphere morphology was prepared by sodium dodecyl benzene sulfonate (SDBS)-assisted solvothermal treatment, exhibiting a stable structure, high conductivity and large specific surface area^[93]. By carbonizing polyacrylamide (PAM) to create a coating, the electronic conductivity of tNVPF was significantly enhanced, resulting in tNVPF@C with exceptional Na⁺ storage capabilities. In addition, a 3D porous carbon was employed as a nucleation substrate to synthesize two-dimensional (2D) NVPF nanosheets (NS) [Na₃V₂(PO₄)₂F₃ nanosheets on 3D porous carbon (NVPF@3Dc)] in a one-step hydrothermal method^[58]. A rapid ion transfer within the a-b plane of the NVPF@3Dc crystal, combined with a minimal volume change during Na insertion and extraction, contributed to enhanced electrode rate performance.

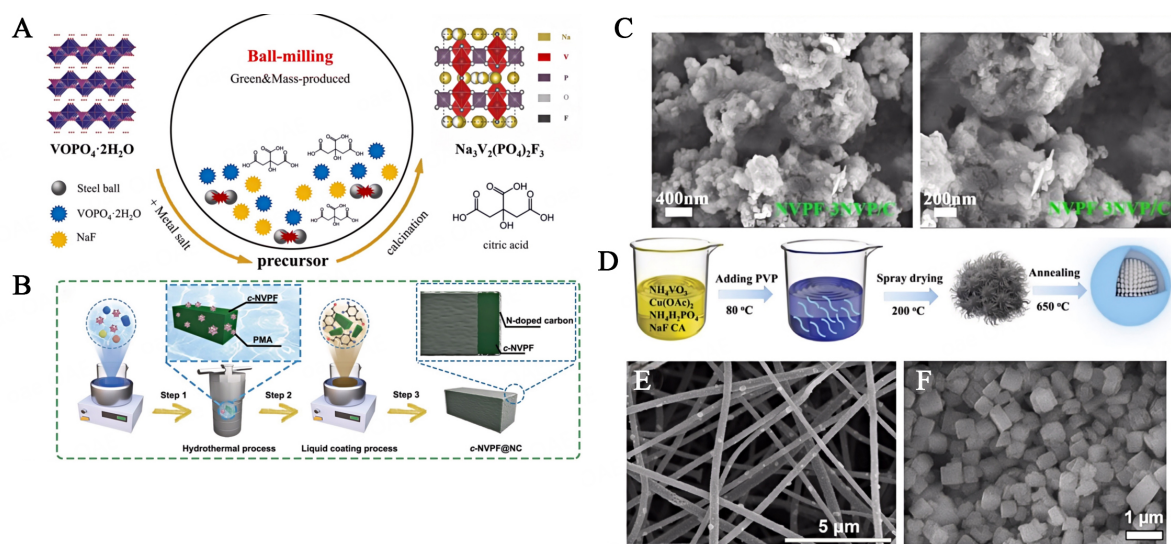


Figure 2. (A) Schematic representation of carbon coated NVPF synthesis by facial ball-milling. Reproduced with permission^[86]. Copyright 2024, Royal Society of Chemistry; (B) Schematic representation of rectangular NVPF synthesis using a hydrothermal method. Reproduced with permission^[90]. Copyright 2023, Wiley -VCH; (C) SEM image of the materials synthesized by the sol-gel technique. Reproduced with permission^[97]. Copyright 2024, Royal Society of Chemistry; (D) Schematic representation of NVPF composite synthesis by spray drying. Reproduced with permission^[102]. Copyright 2024, Wiley; (E) SEM image of the materials synthesized by electrostatic spinning. Reproduced with permission^[105]. Copyright 2023, American Chemical Society; (F) SEM image of the materials synthesized using one-step chemical vapor replacement. Reproduced with permission^[107]. Copyright 2024, Wiley -VCH. NVPF: $\text{Na}_3\text{V}_2(\text{PO}_4)_2\text{F}_3$; SEM: scanning electron microscope.

Hydrothermal/solvothermal methods can enhance reaction rates and generate specific structures, offering significant application potential. However, the synthesis results in variable product morphology and performance. Further research is required to tune the procedure in order to control material uniformity and stability, particularly in large-scale synthesis of NVPF.

Sol-gel method

The sol-gel method represents a simple process, requiring a relatively low reaction temperature, and is widely applied in materials synthesis^[94,95]. Sun *et al.*^[96] have reported a dual-functional N-doped carbon and $\beta''\text{-Al}_2\text{O}_3$ coated NVPF (NC/ $\beta''\text{-Al}_2\text{O}_3$ @NVPF) using the sol-gel procedure with subsequent calcination. The NC/ $\beta''\text{-Al}_2\text{O}_3$ @NVPF cathode exhibited a high capacity (126.7 mAh g^{-1}) at 0.2 C, maintaining 95.5% of capacity after 500 cycles (at 10 C). This response was attributed to compensation for the loss of Na^+ by Na^+ in $\beta''\text{-Al}_2\text{O}_3$ during the formation of the cathode/electrolyte interface film.

Citric acid and oxalic acid are typically used as cross-linking agents and carbon sources in sol-gel synthesis. Yang *et al.*^[97] prepared a carbon-coated $\text{Na}_3\text{V}_2(\text{PO}_4)_2\text{F}_3 \cdot 3\text{Na}_3\text{V}_2(\text{PO}_4)_3$ composite (NVPF-3NVP/C) composite [Figure 2C] where citric acid was employed to fabricate a 3D conductive carbon layer. The synergistic effect of the composites facilitated rapid ionic migration and enhanced the kinetic reactions. Notably, NVP, serving as the primary phase, reinforced structural stability and substantially boosted the capacitive contribution. In a separate study, citric acid was utilized as a chelating agent to synthesize NVPF by sol-gel^[98] where an excess or insufficient chelating agent resulted in F atom deficiency with a loss of crystallinity. It was found that the specific capacity, rate capability, and cycling performance were significantly influenced by the crystallinity of NVPF.

Recent work has considered synergistic strategies involving sol-gel treatment directed at surface modification. For instance, Mahato *et al.*^[99] have provided the first report of rota-tumbler assisted sol-gel to synthesize a series of carbon-coated Fe and Cr co-doped NVPF (NVFCPF). An enlargement in the size of the saddle point, along with the planes of monocapped trigonal prisms and the hexagonal cavities, aided in reducing the ion diffusion activation energy, thereby enhancing the diffusivity of the doped material. In addition, a carboxymethyl cellulose (CMC)-assisted sol-gel strategy was utilized to prepare cross-linked carbon-coated porous NVPF composites (NVPF@C@CMC)^[100]. The CMC provided additional Na⁺ to compensate for sodium loss during the formation of the solid electrolyte interface. Structural stability was enhanced by the cross-linked carbon, and the porous structure of the coating facilitated Na⁺ transfer.

Although the sol-gel method can be used to prepare porous NVPF, additional reaction conditions should be investigated to further improve material pore structure and morphology, such as pH, precursor composition, and temperature.

Spray drying

Spray drying method is commonly used to prepare powder particles or films, offering notable commercial benefits, such as low cost, short processing time, and ease of production. Different morphologies and structures can be achieved by adjusting the preparation conditions and employing auxiliary reagents. For example, a Br-doped spherical NVPF/C was prepared using polytetrafluoroethylene (PTFE) and cetyltrimethylammonium bromide (CTAB) as F supplements and regulators, respectively, in a one-step spray drying procedure^[101]. During the synthesis process, the hard PTFE template supplied additional F, and the resultant porous structure facilitated electrolyte permeation. The soft CTAB template provided Br, and the self-assembly process resulted in a strong spherical structure while refining the particle size. In another study, Zhou *et al.*^[102] synthesized copper substitution NVPF microspheres with an eggshell structure using polyvinyl pyrrolidone (PVP)-assisted spray drying [Figure 2D]. The high electronic conductivity of the cathode material and rapid Na⁺ diffusion were ascribed to the unique eggshell structure and crystal lattice.

Carbon-coated NVPF/carbon nanotube (CNT) nanospheres were synthesized by spray drying followed by calcination^[103]. The 3D CNT network and carbon coated layer enhanced electronic conductivity, increasing the contact area between the cathode and electrolyte, and improving overall the structural stability. Applying sugarcane bagasse as raw material, carbon-coated NVPF nanospheres (NVPF/C) with high capacity were prepared by spray drying combined with high-temperature calcination^[104].

Although the NVPF particles prepared by spray drying exhibited a high degree of uniformity, the structures reported to date are relatively simple, and the ability to control structure by adjusting preparation conditions warrants further investigation.

Electrostatic spinning

Electrostatic spinning involves a relatively simple operation that produces materials with a uniform morphology, and is particularly suitable for synthesizing materials with a one-dimensional linear/tubular structure. These structures can facilitate an oriented transmission of electrons, enhancing reaction kinetics via a conductive network. Electrodes prepared by electrostatic spinning possess a self-supporting structure that serves to increase the specific energy by reducing the use of binders and conductive carbon.

Sodium storage may be improved by adjusting spinning parameters, combined with high-temperature calcination, hydrothermal synthesis, chemical deposition, and other techniques. The porous structure and tubular characteristics can provide channels for Na⁺ transfer, enhancing conductivity. Liang *et al.*^[105] utilized

electrostatic spinning to prepare self-standing NVPF cathodes [Figure 2E]. The NVPF nanoparticles were evenly distributed on the surface and inside the carbon nanofibers (CNFs), which effectively limited particle volume expansion during charging and discharging. Moreover, the CNF network facilitated electron and ion transport. The NVPF self-standing cathode exhibited a high-voltage platform of ~ 4.07 V, and the assembled full cell demonstrated an energy density as high as 185.6 Wh kg^{-1} .

Electrostatic spinning requires stringent experimental conditions as the process is sensitive to temperature and humidity, and involves extended preparation times which have limited large-scale application. In addition, the inorganic fibers produced are susceptible to damage where the fiber length may be significantly decreased during grinding.

Other methods

A number of researchers have considered alternative routes to NVPF materials synthesis. In order to improve the low tap density and poor cycling performance, Song *et al.*^[106] synthesized NVPF materials (HTS-NVPF) with a uniform conductive network and high tap density using a high-temperature shock (HTS) strategy. The ultra-fast high-temperature synthesis (heating rate = $1,100 \text{ }^{\circ}\text{C s}^{-1}$ and heating time = 10 s) circumvented F loss and the formation of impurities, while enhancing cycling stability. The conductive network associated with the large synthesized particles was uniform, contributing to increased conductivity. The HTS-NVPF system exhibited a wide range of operating temperatures ($-45 \text{ }^{\circ}\text{C}$ to $55 \text{ }^{\circ}\text{C}$).

In order to address Na^+ diffusion rate, Wang *et al.*^[107] prepared $\text{Na}_{3-y}\text{VPO}_{2-x}\text{Br}_x\text{F}$ by doping Br^- and pre-loading Na^+ vacancies using a one-step chemical vapor replacement (CVR) method [Figure 2F]. The electrostatically shielded channels in $\text{Na}_{3-y}\text{VPO}_{2-x}\text{Br}_x\text{F}$ reduced coulombic hindrance by Na^+ during the insertion/extraction process, increasing Na^+ diffusion rate by a factor of 5.

A flexible cathode with a high-rate capability and stability can satisfy the requirements of energy storage devices with respect to portability, high power and energy density. A flexible cathode material without binder (NVPF@C/CC) was prepared using a colloidal crystal template method, which anchored nanocarbon onto carbon cloth that was used to coat the NVPF, providing a 3D ordered microporous structure^[108]. The latter facilitated ion diffusion, while the combination of the carbon layer and carbon cloth provided a continuous electronic transmission path, which contributed to a high-rate performance and conductivity.

The electrochemical properties of the NVPF materials synthesized using a range of methods are presented in Table 1.

NVPF MODIFICATION STRATEGIES

It is possible to construct channels for ion transport by regulating the NVPF morphology, which effectively enhances electrochemical performance. Such regulation also serves to reduce the impact of stress on the material volume, and minimize secondary reactions when the electrode contacts the electrolyte. At the nanoscale, the number of active sites on the electrode is increased and the distance for ion diffusion is reduced, which promotes Na^+ diffusion, increasing overall electrochemical activity. The electrochemical properties of materials can be precisely tailored through appropriate modification strategies. Currently, the main modification strategies include carbon coating^[109,110], the use of carbon material composites^[111-114], and elemental doping^[115-124].

Table 1. Electrochemical performance of NVPF cathodes in SIBs prepared using different procedures

Composite	Preparation method	Electrolyte	Electrochemical performances (current density, discharge capacity, cycles, and capacity retention)	Ref.
NVPF@C	solid-state method	EC and DMC (1:1)	20 C, 123 mAh g ⁻¹ , 100, 87.8% (5 C)	[81]
NVPF	carbon thermal reduction method	1 M NaClO ₄ in PC & 5 wt.% FEC	0.1 C, 122 mAh g ⁻¹ , 1,000, 83.2% (10 C)	[84]
NVPF@C-T	solid-state method	1 M NaClO ₄ in EC: DMC: EMC = 1:1:1 with 2 vol.% FEC	0.2 C, 124.5 mAh g ⁻¹ , 300, 94.8% (10 C)	[85]
C-NVPF	surface ball milling method	1 M NaClO ₄ in EC/DEC (1: 1, by vol)	0.1 C, 110.6 mAh g ⁻¹ , 2,000, 54% (5 C)	[86]
NVAPF	ball milling method	1 M NaClO ₄ in PC	0.5 C, 117.4 mAh g ⁻¹ , 100, 92.4% (0.5 C)	[87]
NVPF@rGO	hydrothermal method	1 M sodium NaPF ₆ in diglyme	1 C, 123 mAh g ⁻¹ , 7,000, 85.6% (10 C)	[88]
NVPF/rGO	Hydrothermal /solvent thermal	1 M NaPF ₆ in EC: DEC: DMC (1: 1:1, by vol)	0.1 C, 127 mAh g ⁻¹ , 100, 99% (25 C)	[89]
c-NVPF@NC	hydrothermal method	1 M NaClO ₄ in EC: DMC: EMC (1:1:1) with 5 vol.% FEC	0.2 C, 121 mAh g ⁻¹ , 1,000, 78% (10 C)	[90]
Na ₃ V ₂ (PO ₄) ₂ F ₃	hydrothermal method	2 M NaOH	1 A g ⁻¹ , 168 F g ⁻¹ , 800, 85% (1 A g ⁻¹)	[91]
	solvothermal method	1 M NaClO ₄ in EC: DMC: EMC (1:1:1) with 2 vol.% FEC	0.2 C, 120.7 mAh g ⁻¹ , 300, 80% (5 C)	[92]
NVPF@3Dc	hydrothermal method	1 M NaClO ₄ in EC: PC (1:1) with 2 vol.% FEC	0.2 C, 131.5 mAh g ⁻¹ , 2,500, 64% (5 C)	[58]
NC/β''@NVPF	sol-gel method	1 M NaClO ₄ in EC: DMC: EMC (1:1:1) with 2 vol.% FEC	0.2 C, 126.7 mAh g ⁻¹ , 500, 95.5% (10 C)	[96]
NVPF-3NVP/C	sol-gel method	1 M NaClO ₄ in EC: DEC (1:1, by vol)	0.1 C, 120.7 mAh g ⁻¹ , 200, 64.1% (10 C)	[97]
NVPF	sol-gel method	1 M NaClO ₄ in EC: DEC (1:1, by vol) with 5 vol.% FEC	0.2 C, 112.9 mAh g ⁻¹ , 1,000, 84.6% (5 C)	[98]
NVFCPF	sol-gel method	1 M NaClO ₄ in EC: PC (1:1) with 2 vol.% FEC	0.1 C, 120 mAh g ⁻¹ , 500, 88.6% (1 C)	[99]
NVPF@C@CMC	sol-gel method	1 M NaClO ₄ in EC: DMC: EMC (1:1:1) with 5 vol.% FEC	0.2 C, 125.8 mAh g ⁻¹ , 200, 77% (1 C)	[100]
NVPF/C	spray drying method	1 M NaClO ₄ in EC: PC (1:1) with 5 vol. % FEC	1 C, 116.1 mAh g ⁻¹ , 1,000, 98.3% (10 C)	[101]
NVPF@NC-Cu	spray drying method	1 M NaClO ₄ in EC: PC (1:1) with 5 vol. % FEC	0.1 C, 117.4 mAh g ⁻¹ , 5,000, 91.3% (20 C)	[102]
NVPF/CNTs	spray drying method	1 M NaClO ₄ in EC: PC (1:1) with 5 vol. % FEC	0.1 A g ⁻¹ , 127.7 mAh g ⁻¹ , 20000, 92.1% (10 A g ⁻¹)	[103]
Na ₃ V ₂ (PO ₄) ₂ F ₃ /C	spray drying method	1 M LiPF ₆ in EC: DMC (1: 1, by vol)	0.1 C, 125 mAh g ⁻¹ , 80, 78.23% (0.1 C)	[104]
NVPF	electrostatic spinning method	1 M NaClO ₄ in K1: EC: PC (1:3:6) with 2 vol.% FEC	0.2 C, 101.8 mAh g ⁻¹ , 400, 98.3% (0.2 C)	[105]
HTS-NVPF	high-temperature shock strategy	1 M NaClO ₄ in EC: PC with 5 vol.% FEC	0.1 C, 116.8 mAh g ⁻¹ , 200, 94.2% (1 C)	[106]
Na _{3-y} VPO _{2-x} Br _x F	chemical vapor replacement method	1 M NaClO ₄ in EC: PC (1:1) with 5 vol.% FEC	0.2 C, 124.6 mAh g ⁻¹ , 800, 94.4% (10 C)	[107]
NVPF@C/CC	colloidal crystal template method	1 M NaClO ₄ in EC: DMC (1: 1, by vol)	0.1 C, 118.2 mAh g ⁻¹ , 2,000, 83.3% (20 C)	[108]

NVPF: Na₃V₂(PO₄)₂F₃; SIB: sodium-ion battery; NVPF@C-T: tannic acid-derived carbon-coated Na₃V₂(PO₄)₂F₃; NVPF@C: carbon-coated Na₃V₂(PO₄)₂F₃; EC: ethylene carbonate; FEC: fluoroethylene carbonate; DMC: dimethyl carbonate; EMC: ethyl methyl carbonate; rGO: reduced graphene oxide; C-NVPF: carbon-coated NVPF; c-NVPF@NC: nitrogen-doped carbon-coated Na₃V₂(PO₄)₂F₃; NVPF@3Dc: Na₃V₂(PO₄)₂F₃ nanosheets on 3D porous carbon; NC/β''@NVPF: N-doped carbon and β''-Al₂O₃ coated NVPF; NVPF-3NVP/C: carbon-coated Na₃V₂(PO₄)₂F₃-3Na₃V₂(PO₄)₃ composite; NVFCPF: carbon-coated Fe and Cr co-doped NVPF; CMC: carboxymethyl cellulose; NVPF@NC-Cu: Na₃V₂(PO₄)₂F₃ on nitrogen-doped carbon-coated copper; CNT: carbon nanotube; HTS-NVPF: high-temperature shock Na₃V₂(PO₄)₂F₃; PC: propylene carbonate.

Carbon coated NVPF

One of the key approaches to optimizing electrode structure is to construct an electron transfer system with

high electrical conductivity. It is possible to effectively enhance ion and electron conductivity, and increase electrode stability using surface coating techniques^[125]. Carbon materials are commonly used in coating, offering high conductivity and porous characteristics that provide effective transport channels, increasing electrochemical reaction rates while effectively avoiding direct contact with the electrolyte, which mitigates volume changes during Na⁺ extraction/insertion^[126]. Sun *et al.*^[127] prepared carbon-coated NVPF composites using the sol-gel method, employing PTFE as the carbon source and a fluorine supplement. The presence of the NVP impurity in these carbon-coated NVPF composites was markedly diminished or entirely eradicated.

Carbon-based materials can control NVPF morphology and structure during synthesis and sintering, providing a scaffold that reduces the stress impact caused by electrical effects. Hu *et al.*^[128] have prepared microsphere composite materials (HM-NVPF@CN) assembled from carbon-coated NVPF NS [Figure 3A]. Subsequently, a cathode-electrolyte interface (CEI) layer rich in B and F was constructed on the surface. The unique 2D NS structure of HM-NVPF@CN can shorten the diffusion paths of Na⁺ and e⁻, increasing the reaction contact area while inhibiting parasitic reactions. The thin carbon coating is beneficial for improving electronic conductivity and mitigating structural stress. The optimized electrode exhibited superior cycling stability over a wide temperature range (-25 °C to 60 °C). In addition, NVPF with a porous microsphere structure was synthesized using the deep eutectic solvent method^[129]. The composite carbon coated Na₃V₂(PO₄)₂F₃ microspheres with fluorocarbon layer NVPF/C-F was prepared by forming an amorphous fluoroarbor layer via PTFE surface modification. The study demonstrated that the amorphous fluoroarbor layer promoted Na⁺ diffusion and charge transfer.

Layered carbon materials provide a bridge between electrons and active substances, and effectively promote the migration of Na⁺ between the electrolyte and electrodes. Carbon-coated NVPF with a microcube structure (NVPF/C) was prepared using an open system synthesis method, involving *in situ* growth on graphene oxide (GO) microcubes^[130]. The NVPF/C has an average particle size of ~ 2 μm and a carbon layer thickness of ~ 5 nm. Due to the structure-induced electrochemical reversibility and improved reaction kinetics, it demonstrated the superior electrochemical properties. The carbon coatings prepared *in situ* from inorganic or organic carbon sources exhibit different structural characteristics. For example, carbon-coated NVPF composites were synthesized using branched starch as carbon source and structural template^[131]. Two-dimensional nanostructures were formed where the branched starch induced NVPF nucleation along its main chain. This structural characteristic can shorten the Na⁺ diffusion path and enhance electron transfer.

Carbon coating doped with heteroatoms can significantly improve electronic conductivity and structural stability where the dopants introduce numerous active sites and structural defects, which enhance ion transport efficiency between the electrode and electrolyte. N-doping provides abundant active sites for electrochemical reactions and enhances surface hydrophilicity. An N-doped carbon-coated NVPF composite was prepared using PVP as nitrogen source using the sol-gel method^[132]. The N doping introduced exogenous defects in the carbon layer and additional active sites, increasing conductivity and promoting Na⁺ diffusion.

It is known that dopamine-based coatings can spontaneously accumulate on the surface of the materials. Sun *et al.*^[133] fabricated a bifunctional carbon network by pyrolysis of dopamine (PDA) and PTFE, encapsulating NVPF particles and carbon bridges with an N-doped carbon layer [Figure 3B and C]. The PTFE served to supplement F loss during high-temperature calcination, inhibiting the formation of NVP impurities. The dopamine provided N for the carbon coating layer, creating defects and additional Na

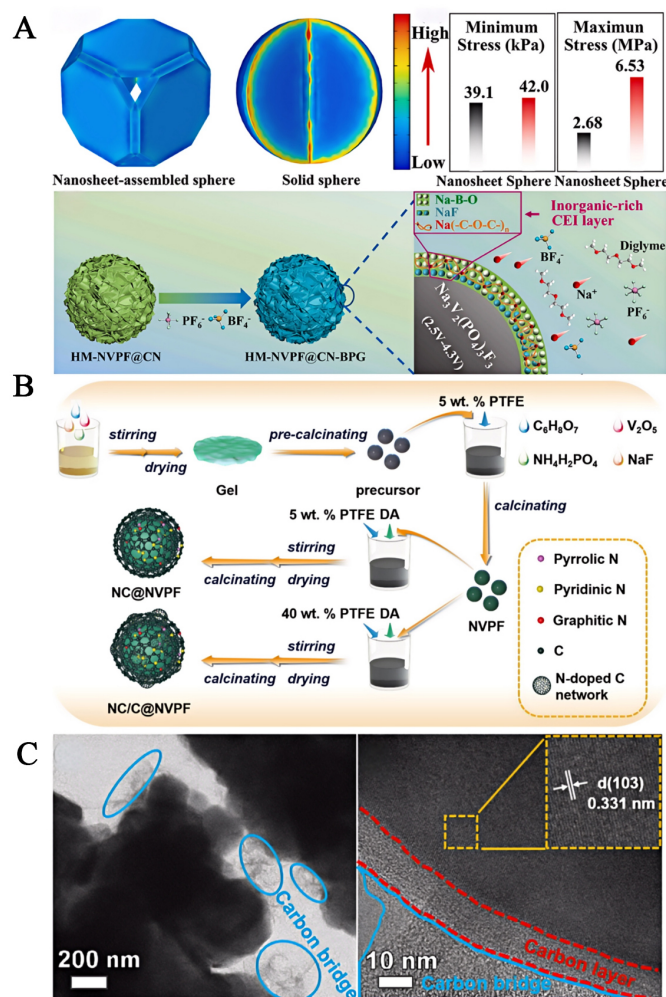


Figure 3. (A) Finite element simulation models and design strategies for NVPF microspheres assembled using carbon coated NVPF nanosheets. Reproduced with permission^[128]. Copyright 2024, Elsevier B.V.; (B) Schematic representation of materials preparation; (C) TEM images of a dual-function carbon network composed of nitrogen-doped carbon layers and carbon bridges. Reproduced with permission^[133]. Copyright 2024, American Chemical Society. NVPF: $\text{Na}_3\text{V}_2(\text{PO}_4)_2\text{F}_3$; TEM: transmission electron microscope.

storage sites. The bifunctional N-doped carbon network can optimize electron/ion transfer at the interface of the electrode material, preventing NVPF corrosion by the electrolyte.

When compared with single atom doping, double atom doping can introduce more active sites, effectively promoting electron and ion transport^[134]. This is particularly the case for doping with N, S, and B, which serves to improve Na⁺ storage capacity and electronic conductivity in diverse modification processes^[135]. In a recent study, a N, B-doped carbon-coated NVPF composite (NVPF@NBC) was prepared by a mechanical ball-milling assisted sol-gel procedure, employing polyacrylonitrile (PAN) and boric acid as nitrogen and boron sources, respectively^[136]. The co-doping of N and B atoms increased the number of defects in the carbon, enhancing Na⁺ storage and transport. The N, B co-doped carbon layer can reduce particle agglomeration and maintain structural stability. Yu *et al.*^[137] synthesized a N/B co-doped carbon coated NVPF (NVPF-CNB) using the sol-gel method with 1-vinyl-3-methyl imidazole tetrafluoroborate as the nitrogen and boron source, and a carbon-coated NVPF composite using ionic liquid-acrylic copolymer as a modification reagent^[138]. A N/S co-doped carbon-coated NVPF (NVPF@NSC) was also prepared by sol-gel

combined with mechanical ball-milling which employed thiourea as the nitrogen and sulfur source^[139]. The study revealed that the doping of N and S had no impact on the crystal structure of NVPF, but demonstrated excellent reversibility and minimal polarization.

Despite the widespread use of carbon-coated NVPF composite materials, graphitization in carbon layers remains a challenge that impairs electronic conductivity. Moreover, it is difficult to form uniform carbon layers using current preparation procedures, which has a significant impact on Na⁺ migration between particles and electrolytes. It should also be noted that carbon layers formed from different carbon sources have varying electrochemical properties. Preparation conditions and the use of regulatory factors warrant further investigation.

Carbon composite NVPF

When NVPF particles experience fracture or loss of potential contact, the resistance between them intensifies, resulting in decreased capacity. It is essential to construct a stable NVPF structure and maintain a consistent and reliable electrochemical output. Three-dimensional conductive carbon materials, notably CNTs, are recognized as the most suitable candidates for this purpose. Research has conclusively demonstrated the efficacy of CNTs in boosting ionic transport^[140]. By embedding CNTs within NVPF particles and constructing an interconnected network, the material can better accommodate Na⁺ volumetric fluctuations during repeated charging and discharging, maintaining the electrical conductivity between self-assembled particles. For example, Ma *et al.*^[141] synthesized a CNT-hybrid dual-phase anionic phosphate material (denoted as NFC) via a one-pot sintering method. The material consisted of NVPF with interwoven CNTs and a minor amount of NVP. This cathode material demonstrated a wide operating temperature range (-20 °C to 50 °C). A NVPF@CNT composite was prepared by anchoring NVPF nanoparticles on CNTs with a low number of walls [Figure 4A-C]^[142]. Ion transmission via the CNTs promoted the growth of primary NVPF crystal particles. The high crystallinity and anchoring effect enhanced structural stability, while the 3D network composed of CNTs and amorphous carbon layers increased conductivity. This strategy can improve material crystallinity and increase grain size. CNTs were utilized as an effective medium to adjust the electronic conductivity of NVPF in a recent study^[143].

Research has shown that the formation of a 3D cross-linked carbon network can enhance charge transfer kinetics and shorten the ionic transfer pathway. For instance, a composite with a cross-linked dual-carbon framework structure [Na₃V₂(PO₄)₂F₃ caged in 3D cross-linked carbon networks composed of carbon layer and intertwined CNTs (NVPF@C@CNTs)] was constructed by cross-linking NVPF with amorphous carbon and CNTs^[144], and NVPF@C/CNTs composites with a carbon-coated 3D conductive network were prepared by solvothermal method^[145].

Introducing graphene is an effective strategy to improve electrode performance. GO can serve as an efficient carrier for immobilizing nanoparticles due to its unique 2D structure^[146,147]. A high-temperature heat treatment is used to prevent particle agglomeration and lower the GO content with a stable anchoring of NVPF, and an extended contact area between the electrode and electrolyte^[148]. For instance, NVPF-gel/rGO composites were synthesized using a hydrothermal procedure with addition of gelatin and rGO^[149]. The morphology of the material exhibited a high degree of uniformity where the addition of gelatin reduced impurities, and the presence of graphene enhanced Na⁺ diffusion [Figure 4D and E]. Shi *et al.*^[150] prepared a composite material (NVPF@rGO/CNT) by self-assembly, generating a 3D cross-linked conductive network containing 2D rGO and 1D CNT [Figure 4F], which makes it feasible to operate in a wide temperature range (-40 °C to 50 °C).

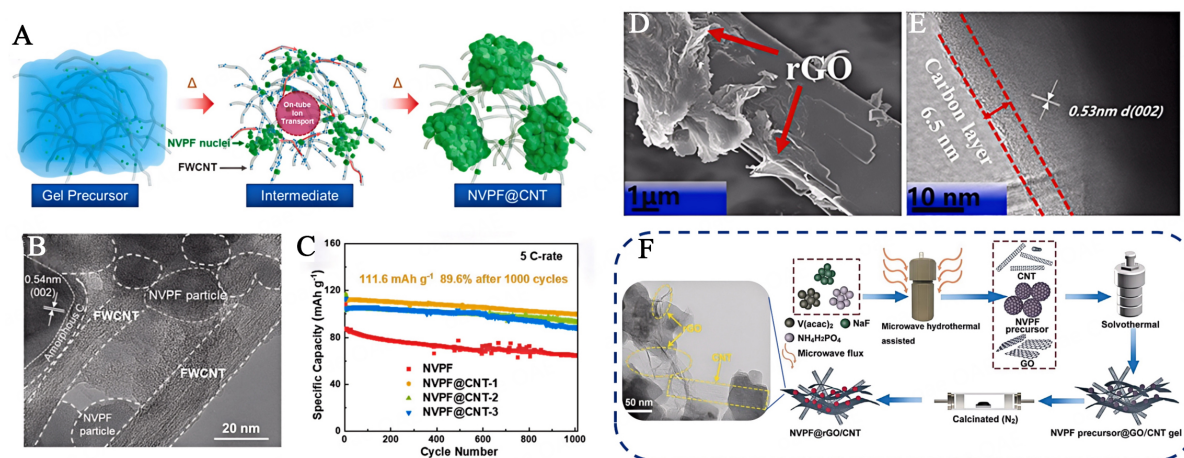


Figure 4. (A) Schematic representation of ion transport by CNTs to promote NVPF grain growth; (B) Synthesis process of NVPF@CNT composite materials; (C) Cycle performance of different materials. Reproduced with permission^[142]. Copyright 2023, Elsevier; (D) SEM and (E) HRTEM images of NVF-GEL/rGO. Reproduced with permission^[149]. Copyright 2022, Elsevier. (F) Schematic representation of the synthesis process. The illustration is TEM image of NVPF@rGO/CNTs. Reproduced with permission^[150]. Copyright 2023, Wiley. CNT: Carbon nanotube; NVPF: $\text{Na}_3\text{V}_2(\text{PO}_4)_2\text{F}_3$; NVPF@CNT: $\text{Na}_3\text{V}_2(\text{PO}_4)_2\text{F}_3$ coated with carbon nanotubes; SEM: scanning electron microscope; HRTEM: high resolution transmission electron microscope; NVF-GEL/rGO: NVPF modified reduced graphene oxide using GEL method.

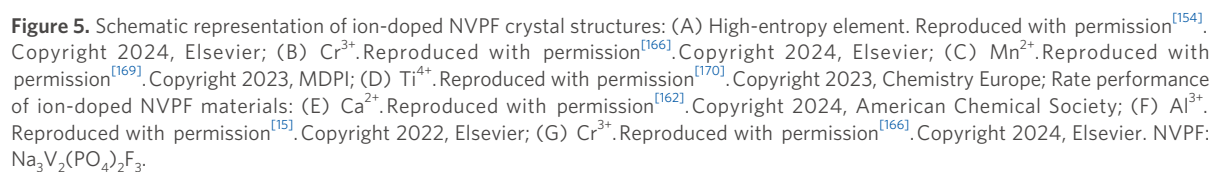
Combining conductive carbon with NVPF is an effective strategy to enhance electronic conductivity. This is particularly the case when the carbon materials form 3D or dual-carbon layer wrapping structures.

Element doping of NVPF

NVPF materials typically exhibit lower intrinsic electronic conductivity and limited rate performance due to the insulating properties of the $[\text{PO}_4]$ tetrahedron. Element doping enables a flexible adjustment of material properties, such as electronic conductivity, structural defects, crystallinity, and redox potential. The doping elements can be classified into three categories based on differences in the substitutional sites: sodium ion site substitution; vanadium ion site substitution; anion site substitution. Recent research has mainly focused on the first two types of substitution.

Doping elements with a larger ionic radius at the Na site in NVPF materials can lead to an increase in lattice spacing that, in turn, widens the channels for ionic diffusion^[151,152]. This ensures that the NASICON framework is not damaged or affected by internal stress and structural deformation during charge and discharge cycles. Moreover, the introduction of these elements results in a shortening of the vanadium-fluorine bond (V-F) and vanadium-oxygen bond (V-O) bond lengths in the lattice, enhancing NVPF structural stability. Wu *et al.*^[153] have prepared composite materials with a carbon coating by the sol-gel method, incorporating K^+ to replace a Na^+ component in NVPF crystals [carbon coated $\text{Na}_3\text{V}_2(\text{PO}_4)_2\text{F}_3$ doped with K^+ ($\text{Na}_{1-x}\text{K}_x\text{V}_2\text{PF}_3/\text{C}$)]. The doped K^+ , which was located at the Na1 site, did not participate in reaction during charge-discharge, ensuring high Na^+ migration. The doping of K^+ reduced the bandgap energy and increased electronic conductivity.

The introduction of high-entropy elements (Mg, Cr, Al, Nb) can improve the stability of the Na2 site in NVPF, and suppress the intermediate reaction of the NVPF phase at low potentials. High-entropy carbon-coated NVPF composites (NVPF-HE@C) [Figure 5A], synthesized by the sol-gel method, exhibited a significant improvement in the specific capacity, capacity retention, and Na^+ diffusion coefficient^[154]. Doping with Fe serves to refine the particles, inhibiting particle agglomeration, and promoting Na^+



When compared to doping at the Na site, the method of replacing V with inexpensive elements represents a more common approach that can reduce the toxicity due to V and lower overall costs. Inactive elements (such as Mg^{2+} ^[156,157], Al^{3+} ^[158,159], and Y^{3+} ^[117]) that do not participate in electrochemical reactions, can promote the formation of defects in the NVPF crystals, providing additional charge transfer pathways.

The holes that are generated by the substitution of V by Mg enhance conductivity. The Mg^{2+} dopant does not participate in redox reactions, but can suppress changes to the lattice structure. Wang *et al.*^[160] prepared a NVPF composite $[\text{Na}_{3.3}\text{K}_{0.2}\text{V}_{1.5}\text{Mg}_{0.5}(\text{PO}_4)_2\text{F}_3]$ with N-doped carbon coating, employing a binary co-doping strategy. The surface of the N-doped carbon layer was rich in defects, providing additional active sites and enhancing conductivity. Such modifications accelerate the reaction kinetics and augment electrolyte interaction through an expanded specific surface area, thus streamlining the electrochemical process. Concurrently, strategic heteroatom substitution leads to a more efficient engagement of Na^+ in the electrochemical activities, thereby bolstering the cathode's structural integrity. The ionic radius of Bi^{3+} is larger than that of V, which is beneficial for Na^+ intercalation by increasing the interplanar spacing. A Bi-doped carbon-coated NVPF $[\text{Na}_3\text{V}_{2-x}\text{Bi}_x(\text{PO}_4)_2\text{F}_3/\text{C}]$ was synthesized using the sol-gel method combined with high-temperature calcination^[161]. The results indicate that the incorporation of an optimal amount of Bi-doping and carbon coating significantly enhanced the conductivity, Na^+ diffusion performance, and structural stability of the cathode material during the charge-discharge cycle.

Replacing V^{3+} with Ca^{2+} can reduce the bandgap, enhance electronic conductivity, and improve structural stability. Puspitasari *et al.*^[162] prepared a Ca-doped NVPF cathode material with a carbon coating [Ca-doped $Na_3V_2(PO_4)_2F_3$ with a carbon coating (NVPF-Ca-x/C)] using sol-gel and carbothermal reduction techniques. The results have shown that Ca^{2+} doping did not alter the crystal structure but expanded the lattice spacing. The incorporation of the Ca^{2+} ion leads to the emergence of two localized states within the band gap, thereby significantly improving the electrochemical performance in comparison to Mg-doped NVPF/C.

Doping trivalent rare-earth ions at the V^{3+} site is an effective strategy for improving NVPF performance. In a recent study, an atomic simulation method based on the minimization of lattice energy was used to explore the effects of rare-earth ion doping on the local structural deformation and intrinsic defect properties of the NVPF cathode material^[163]. The study found that defects formed by Na interstitials and vacancies (Na Frenkel defects) serve to promote Na^+ diffusion. In addition, the concentration of Na vacancies and interstitials can be increased by doping rare-earth ions at Na and P sites, enhancing reaction kinetics.

The removal or insertion of excess Na^+ in NVPF can be achieved within a relatively wide voltage range by adding Al. A study of Al-doped NVPF (NVAIPF-x) synthesis has demonstrated that Al doping reduced the band gap without causing a phase transition^[15]. Doping with Al increased the Na^+ diffusion coefficient, and Al^{3+} successfully replaced the V^{3+} site within the NVPF lattice.

A high-entropy doping can suppress adverse phase transitions at low voltages, promoting Na^+ storage at high voltages. Gu *et al.*^[60] have applied the concept of high entropy with respect to the PACs lattice, and prepared a carbon-free high-entropy $Na_3V_{1.9}(Ca,Mg,Al,Cr,Ca)_{0.1}(PO_4)_2F_3$ cathode material by partially substituting V atoms. Density functional theory (DFT) calculations have shown that high-entropy doping alters the electronic state, enhancing conductivity and Na^+ migration rate, further elevating the average voltage platform to 3.81 V and increasing the energy density to 445.42 Wh kg^{-1} .

During the electrode reaction, new active redox pairs can be formed by high-activity elements, such as Mn^{2+} ^[164], Cr^{3+} ^[118], and Ti^{3+} ^[63], which serve to appreciably enhance the specific capacity and output voltage^[165]. Chromium doping is particularly effective as Cr^{3+} has a similar ionic radius to V^{3+} . A moderate level of Cr^{3+} doping can introduce crystal defects, reducing the Na^+ transport distance, and enhancing diffusion with higher electron transfer and charge transfer rates. For instance, Cr-doped NVPF composites with a carbon coating were synthesized using Cr^{3+} as an iso-valent doping ion by the sol-gel method^[166] [Figure 5B]. The results established improved electrical conductivity as a result of lower charge transfer resistance (R_{ct}) due to Cr^{3+} doping. In addition, Yi *et al.*^[167] prepared Cr-doped NVPF composites [$Na_3V_{2-x}Cr_x(PO_4)_2F_3/C$] by sol-gel. The enhanced electrochemical performance is attributed to the elevated crystallinity, optimized intrinsic electronic conductivity, and Na^+ diffusion coefficient resulting from the doping of Cr^{3+} . This doping accelerates the electron transport and charge transfer rate.

An appropriate level of Mn^{2+} incorporation in NVPF can effectively enhance the Na^+ diffusion rate due to the larger radius of Mn^{2+} relative to V^{3+} that regulates the lattice and surface energy. Gu *et al.*^[168] synthesized NVPF-NS with a 2D NS structure, which enabled an adjustment of the surface energy and V site in NVPF by partially replacing V^{3+} with Mn^{2+} . This led to combined presence of V^{3+} and V^{4+} , which enhanced NVPF electronic conductivity and structural stability. NVPF materials doped with different valence Mn ions have been produced in a hydrothermal procedure^[169]. The results reported demonstrated that Mn doping altered the NVPF crystal structure and residual carbon content [Figure 5C]. The incorporation of Mn^{2+} resulted in a NVPF micro-rectangular morphology, restricting crystal size, reducing R_{ct} and promoting Na^+ diffusion.

Doping with Ti can effectively inhibit the formation of an irreversible tetragonal phase, and achieve Na⁺ storage via a reversible transition from the *Amam* to *Cmc21* phase. Tong *et al.*^[170] synthesized Ti-doped NVPF (NVTPF) cathode material by solid-state sintering [Figure 5D]. The incorporation of Ti stabilized the local structure via F-Ti bond formation by precipitation, with minimal changes during charge and discharge. In the electrochemical process, vanadium was reversibly transformed from V³⁺ to V⁵⁺, where Ti⁴⁺ was unchanged. The substitution of W⁶⁺ at the V site can improve Na⁺ diffusion and electronic conductivity, while inhibiting grain growth. W-doped carbon-coated NVPF synthesis using a sol-gel and ball-milling assisted by sonication has been shown to enhance structural integrity and improve Na⁺ mobility^[171].

The element-doped NVPF with excellent rate performance reported in recent studies is illustrated in Figure 5E-G. A comparison of the electrochemical performance of NVPF cathodes in SIBs prepared using different doping strategies is presented in Table 2. It is evident that ion doping can enhance the intrinsic conductivity of NVPF, maintaining the stability of the crystal structure. Doping with inexpensive metals can reduce production costs. However, the incorporation of ions with large radii and excessive doping may damage the crystal structure and lower material stability. In order to ensure effective doping, many factors such as element type, doping amount, distribution uniformity, dopant siting and cost require further comprehensive investigation.

OPTIMIZATION OF SIBS

Researchers have employed a number of strategies to enhance the electrochemical performance of NVPF in SIBs, such as interface and defect engineering^[172], adjustment of the electrode structure^[173,174], and optimization of electrolyte composition^[175-177]. The associated mechanisms that underpin electrochemical performance have also been investigated.

Interface and defect engineering

In recent years, researchers have made numerous attempts to improve NVPF electrochemical performance by utilizing interface and defect engineering to enhance electronic transmission dynamics and ionic diffusion kinetics, mitigating the structural stress generated during electrochemical processes.

Defect engineering can optimize Na⁺ transport kinetics. By introducing ordered vacancies, Na⁺ can be uniformly adsorbed, alleviating mechanical stress during charging and discharging and significantly improving rate performance^[178]. Bulk nitrogen doping in NVPF can expand the interlayer spacing and enhance electronic conductivity, raising the voltage platform while achieving ultra-long cycle stability^[179]. Vacancies or doping defects can lower the migration energy barrier for sodium ions and increase the diffusion coefficient.

Interfacial engineering can enhance structural stability and interface compatibility. The construction of strong chemical bond interfaces can inhibit surface side-reactions and improve electron transport efficiency^[180]. Hard carbons are the most commonly used anode materials in SIBs, while they generally suffer from poor cycling and rate capability. Glyme-ether-based electrolytes enable long-term cycling of SIBs based on hard carbon anode and NVPF cathode, due to the formation of fluorine-rich SEI layer with superior stability^[181]. Applying carbon coating or compositing with conductive materials (such as graphene) reduces interface impedance and alleviates volume expansion, improving the cycling stability of NVPF^[103,108,128,145,150].

Interface and defect engineering can significantly improve the rate performance, cycle life, and low-temperature adaptability of NVPF cathodes by regulating Na⁺ transport pathways, enhancing electronic

Table 2. Comparison of the electrochemical performance of NVPF cathodes in SIBs prepared using different elemental doping strategies

Composite	Doped element	Electrolyte	Electrochemical performances (current density, discharge capacity, cycles, and capacity retention)	Ref.
$N_{1-x}K_xVPF/C$	K	1 M $NaClO_4$ in EC: PC (1:1) with 5 vol.% FEC	0.2 C, 128 mAh g^{-1} , 100, 92% (0.2 C)	[153]
NVPF-HE@C	high-entropy elements (Mg, Cr, Al, Nb)	1 M $NaClO_4$ in EC/PC	1 C, 128 mAh g^{-1} , 800, 83% (5 C)	[154]
Fe-NVPF@N-CNTs	Fe	1 M $NaClO_4$ in DEC:EC = 1:1 vol% with 5 % FEC	0.1 C, 105 mAh g^{-1} , 1,200, 83.38% (5 C)	[155]
$Na_{3.3}K_{0.2}V_{1.5}Mg_{0.5}(PO_4)_2F_3$	K, Mg	1 M $NaClO_4$ in EC: DMC: DEC (1:1:1, vol)	1 C, 115.6 mAh g^{-1} , 1,000, 93.1% (10 C)	[160]
$Na_3V_{2-x}Bi_x(PO_4)_2F_3/C$	Bi	1 M $NaClO_4$ in EC: DEC (1:1) with 5 vol.% FEC	0.1 A g^{-1} , 107.4 mAh g^{-1} , 100, 90.4% (0.1 A g^{-1})	[161]
NVPFCa-x/C	Ca	1 M $NaClO_4$ in EC: PC (1:1, by vol)	0.1 C, 124 mAh g^{-1} , 1,000, 70% (10 C)	[162]
NVAIPF-x	Al	1 M $NaClO_4$ in EC: DEC (1:1) with 5 vol.% FEC	0.1 C, 121.3 mAh g^{-1} , 400, 75% (5 C)	[15]
$Na_3V_{2-x}Cr_x(PO_4)_2F_3/C$	Cr	1 M $NaClO_4$ in PC with 5 vol. % FEC	0.2 C, 117 mAh g^{-1} , 1,000, 68.7% (10 C)	[167]
NVPF-NS	Mn	1 M $NaClO_4$ in PC with 5 vol. % FEC	0.1 C, 120 mAh g^{-1} , 1,000, 80.7% (1 C)	[168]
NVMPF@C	Mn	1 M $NaClO_4$ in EC: DMC (1:1) with 5 vol.% FEC	0.2 C, 116.2 mAh g^{-1} , 400, 67.7% (1 C)	[169]
NVTPF	Ti	NaPF6 in PC/EC/DMC (1:1:1, by vol)	0.1 C, 70 mAh g^{-1} , 100, 90% (0.1 C)	[170]
NVPFW	W	1 M $NaClO_4$ in EC: PC (1:1, by vol) with 3 vol.% FEC	0.1 C, 140 mAh g^{-1} , 250, 97.4% (2 C)	[171]

NVPF: $Na_3V_2(PO_4)_2F_3$; SIB: sodium-ion battery; $N_{1-x}K_xVPF/C$: carbon coated $Na_3V_2(PO_4)_2F_3$ doped with K⁺; EC: ethylene carbonate; PC: propylene carbonate; FEC: fluoroethylene carbonate; NVPF-HE@C: high-entropy carbon-coated NVPF composites; Fe-NVPF@N-CNTs: Fe-doped $Na_3V_2(PO_4)_2F_3$ coated by N-doped CNTs; NVPFCa-x/C: Ca-doped $Na_3V_2(PO_4)_2F_3$ with a carbon coating; NVAIPF-x: Al-doped $Na_3V_2(PO_4)_2F_3$; NVPF-NS: $Na_3V_2(PO_4)_2F_3$ with a nanosheet structure induced by partially replacing V^{3+} with aliovalent Mn^{2+} ; NVMPF@C: carbon coated $Na_3V_2(PO_4)_2F_3$ doped with Mnx^{+} ; DMC: dimethyl carbonate; NVTPF: Ti-doped $Na_3V_2(PO_4)_2F_3$; NVPFW: W-doped $Na_3V_2(PO_4)_2F_3$.

conductivity, and optimizing interface stability. Future research should focus on a precise design of defects and interfaces, with an examination of synergistic optimization mechanisms.

Optimization of electrolyte composition

The electrolyte provides the necessary medium for ionic transfer between cathode and anode^[182]. There are currently two main approaches to optimizing SIB electrolytes. The first deals with ionic conductivity and viscosity, focusing on the type or composition of the electrolyte. The second considers the use of electrolyte additives to form a stable protective layer at the interface between the electrolyte and the electrode, enhancing battery cycling performance.

The operation of SIBs at temperatures above 50 °C presents challenges in terms of safety and stable cycling, requiring high-temperature-resistant liquid electrolytes. Liang *et al.*^[183] combined fluoroethylene carbonate (FEC) and trimethylsilyl phosphite (TMSPi) to prepare a non-flammable electrolyte. This dual-functional integrated strategy resulted in a non-combustible electrolyte with thermal stability that ensured safe and stable battery operation at high temperatures [Figure 6A and B]. In addition, the same research group considered a film-forming modulation strategy, which improved the ionic transport capability and structural/thermal stability of CEI/SEI (solid electrolyte interphase) by optimizing the interfacial formation of P/Si intermediates, enabling stable operation of the SIB over a wide temperature range (-25 °C to 75 °C),

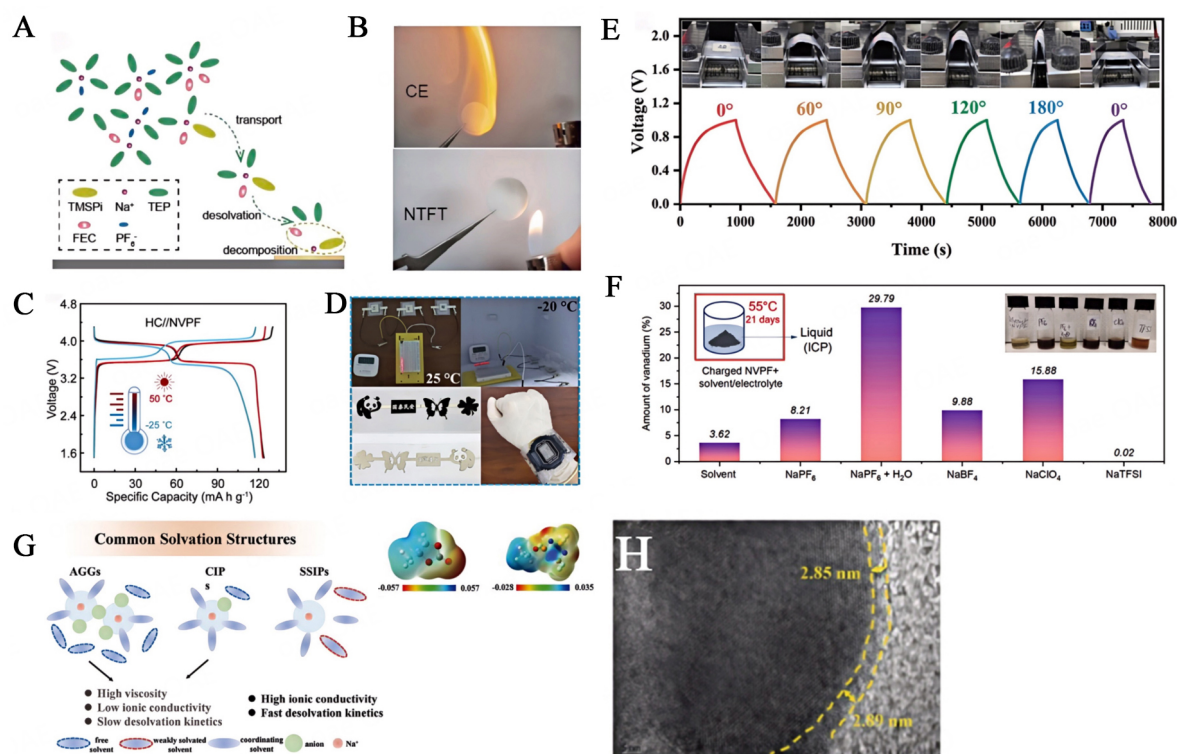


Figure 6. (A) The TMSPI-induced film formation process; (B) Flame test carried out with separators soaked in different electrolytes. Reproduced with permission^[183]. Copyright 2024, Elsevier; (C) Galvanostatic charge-discharge (GCD) curves associated with continuous temperature testing simulating a wide range of all-weather conditions. Reproduced with permission^[184]. Copyright 2024, American Chemical Society; (D) Power to electronic devices at 25 °C and -20 °C; (E) GCD curves of a battery with different bending angles at 0.1 C. Reproduced with permission^[185]. Copyright 2024, Wiley; (F) V dissolution of a charged NVPF powder in EC-PC-DMC with different sodium salts at 55 °C for 21 days. Reproduced with permission^[186]. Copyright 2023, Elsevier; (G) Schematic representation of solvation structure; (H) TEM image of a circulating NVPF cathode in NPP6 electrolyte (PFPN as a co-solvent in electrolyte at molar ratio of PC:PFPN = 7.5:1). Reproduced with permission^[188]. Copyright 2024, Wiley -VCH. TMSPI: trimethylsilyl phosphite; NVPF: Na₃V₂(PO₄)₂F₃; EC: ethylene carbonate; PC: propylene carbonate; DMC: dimethyl carbonate; TEM: transmission electron microscope; NPP6: 6th sodium-ion electrolyte formulation with PC and PFPN; PFPN: ethoxy (pentafluoro) cyclotriphosphazene.

successfully achieving all-weather adaptability [Figure 6C]^[184]. The assembled HC//NVPF full cell maintained over 90% capacity retention following long-term testing at -25 °C and 50 °C. The addition of an organic co-solvent can improve the low temperature resistance of the battery. A fully-printed flexible aqueous rechargeable SIB (ARSIB) with superior mechanical properties was assembled using screen printing technology for the first time, with NVPF/C as the cathode material and Na₃MnTi(PO₄)₃/C as the anode material^[185]. A 17 m (mol kg⁻¹) NaClO₄-EG mixed electrolyte which can withstand low temperature (-20 °C) was prepared by incorporating ethylene glycol (EG) as co-solvent with the 17 m NaClO₄ electrolyte. This flexible battery had a capacity of 40.1 mAh g⁻¹, with outstanding mechanical and cycling performance [Figure 6D and E].

The dissolution of V and resultant parasitic reactions are widely recognized as key factors leading to declining battery performance. A combined use of surface coatings and changes in electrolyte formulation was proposed to reduce V dissolution [Figure 6F]^[186]. It was shown that electrolytes based on sodium trifluoromethane sulfonimide (NaTFSI) inhibited V dissolution, but degradation must be prevented at high potentials. In addition, a carbon coating of NVPF particles with the addition of electrolyte surface protective agents is effective in minimizing V dissolution.

The formation of an anion-derived CEI layer improves interfacial stability and promotes rapid transfer of Na^+ at the interface. The NVPF cathode exhibited greater stability in the diglyme-based electrolyte. Zheng *et al.*^[187] have reported a thorough examination of the Na storage mechanism by NVPF in diglyme and propylene carbonate(PC)/ethylene carbonate (EC) electrolytes containing 0.5 M NaPF_6 at low temperatures. This electrolyte system significantly enhanced the rate of Na^+ diffusion in the bulk electrolyte with a reduction in the charge transfer barrier to 158.6 meV, which is only one-third of that in a PC/EC-based electrolyte. Moreover, the battery can function normally and maintain stable performance at -60°C .

Recently, a novel ternary low-concentration electrolyte and cation/anion solvation strategy was proposed, which utilized ethoxy (pentafluoro) phosphazene (PFPN) as a weakly polar solvent to improve the electrode/electrolyte interfacial stability and enhance ion conductivity and oxidation stability [Figure 6G and H]^[188]. This strategy enabled increased cycling performance and energy density, facilitating durable high-voltage SIBs. The ionic conductivity of the low-concentration electrolyte was increased to 6.12 mS cm^{-1} , and the electrochemical stability window was raised to 4.84 V.

The fundamental cause of the significant capacity decline of NVPF_3 -based batteries is associated with the continuous electrolyte oxidation process rather than F loss or the collapse of the crystal structure. The capacity retention of NVPF_3 batteries can be improved by optimizing the electrolyte. Jiang *et al.*^[189] designed an electrolyte additive containing two $-\text{C}\equiv\text{N}$ groups that enabled a stable SIB cycling at high voltage.

Sulfonate anion-based ionic liquids have been widely used as electrolytes for secondary batteries. An inhibitory effect of the $\text{Na}[\text{FSA}]-[\text{C}_2\text{C}_1\text{im}][\text{FSA}]$ ionic liquid on Al corrosion in the presence of $[\text{FAP}]^-$ has been reported^[190]. A uniform deposition passivation layer formed by the decomposition products of $[\text{FSA}]^-$ and $[\text{FAP}]^-$ mitigated the corrosion of Al after adding $[\text{FAP}]^-$. The study found that $\text{Na}[\text{FSA}]-[\text{C}_2\text{C}_1\text{im}][\text{FSA}]$ moderately inhibited Al corrosion at 25°C , but a severe pitting corrosion of the Al electrode was observed at 90°C when the potential was higher than 4 V vs Na^+/Na . In the charge-discharge tests of NVPF electrodes, the addition of $[\text{FAP}]^-$ elevated the electrochemical performance of the ionic liquid electrolyte, particularly at high temperatures.

Exogenous additives

Strategies for increasing the exposure of active crystal facets that promote Na^+ transport involving selective crystal growth are crucial to developing cathodes for high-performance SIBs^[191]. For example, NVPFs with different (002) face exposure rates were synthesized using carbon clusters (c-clusters) as inducers to regulate the surface energy [Figure 7A]^[192]. The study demonstrated that the (002) face possessed more stable Na^+ storage sites and lower diffusion barriers, where the adsorption of c-clusters generated 2D particles that influenced the crystal growth direction. The optimized NVPFs exhibited a high reversible capacity (123 mAh g^{-1}) and energy density (431 Wh kg^{-1}).

Chemical pre-precipitation (CP) is an effective method to enhance SIB energy density. Current sodium agents are mostly polycyclic aromatic hydrocarbons with low reduction potential, which can readily result in excessive sodium insertion in the cathode with structural deterioration. As novel CP agents, aromatic ketones can endow the agents with mild reducibility by introducing the carbonyl ($\text{C}=\text{O}$) function to balance conjugation and inductive effects [Figure 7B]^[193]. While maintaining structural stability, the charge capacity of the positive electrode material was significantly improved.

Introducing a sodium polyacrylate (NaPAA) binder to the NVPF cathode can overcome the instability of the interface^[194]. The NaPAA binder interacted with the NVPF cathode via ionic-dipole interactions,

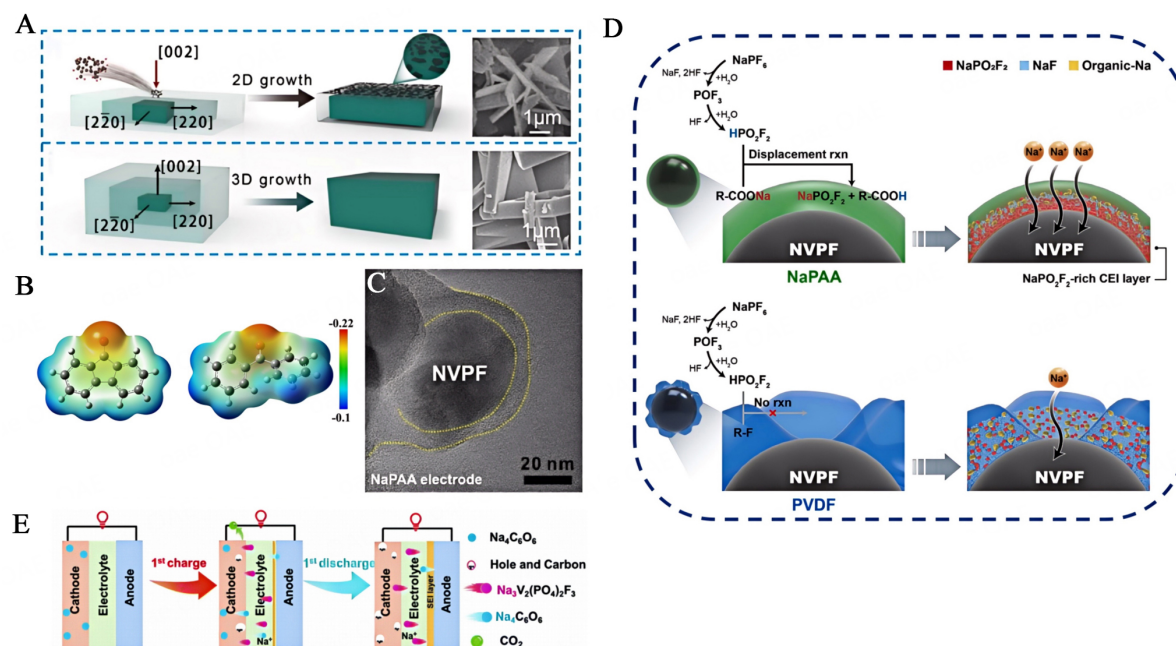


Figure 7. (A) Schematic representation of NVPF growth. Reproduced with permission^[192]. Copyright 2024, Royal Society of Chemistry; (B) Electron cloud density of associated materials. Reproduced with permission^[193]. Copyright 2024, Wiley -VCH; (C) TEM image of NVPF particle; (D) Schematic representation of the effects of NaPAA and PVDF binders on the formation of CEI layers. Reproduced with permission^[194]. Copyright 2024, Royal Society of Chemistry; (E) Schematic representation of the Na₄C₆O₆ loss compensation mechanism for the cathode and anode. Reproduced with permission^[195]. Copyright 2022, Royal Society of Chemistry. NVPF: Na₃V₂(PO₄)₂F₃; TEM: transmission electron microscope; NaPAA: sodium polyacrylate; PVDF: polyvinylidene fluoride; CEI: cathode-electrolyte interface.

improving the distribution of active materials and forming a stable ionic conductive NaPO₂F₂-rich CEI layer that effectively inhibited electrolyte decomposition [Figure 7C and D]. Zhang *et al.*^[195] prepared a novel high-capacity self-sacrificial Na₄C₆O₆ additive, which contained a large number of sulfonic carboxyl groups [Figure 7E]; the resultant capacity exceeded 400 mAh g⁻¹. This additive can provide sufficient Na to compensate for Na loss during the initial charge-discharge cycle. The energy density of the full cell with 9% additive (HC//NVPF/rGO) increased from 154.5 Wh kg⁻¹ to 210.8 Wh kg⁻¹.

Mechanism of SIB performance

As the battery interphase properties and chemical composition vary with temperature and the dissolution and recombination of the interphase are affected by temperature, the desired characteristics can be achieved by combining high and low temperatures. A recent study has illustrated the effect of temperature on the interphase properties of Na₃V₂(PO₄)₂F₃/hard carbon (NVPF|HC) batteries [Figure 8A]^[196]. The results demonstrated that cycle stability, impedance, and rate performance were sensitive to temperature, leading to different SEI formation pathways. The battery capacity retention and coulomb efficiency values were lowest at 25 °C. At higher temperatures, the battery was stable but exhibited a high impedance, whereas the NaF content was high with minimal transition metal dissolution at low temperatures. Superior reversible capacity, cycle stability, and high-power rate capability can be achieved by adjusting temperature.

Komayko *et al.*^[197] investigated the effects of two different intercalation approaches on the performance of SIB cathode materials at low temperatures and high discharge current limits [Figure 8B]. The research established that NaVPO₄F, which followed a solid solution mechanism, was significantly superior to NVPF which exhibited phase separation during Na⁺ intercalation. The energy density retention of NaVPO₄F at 10

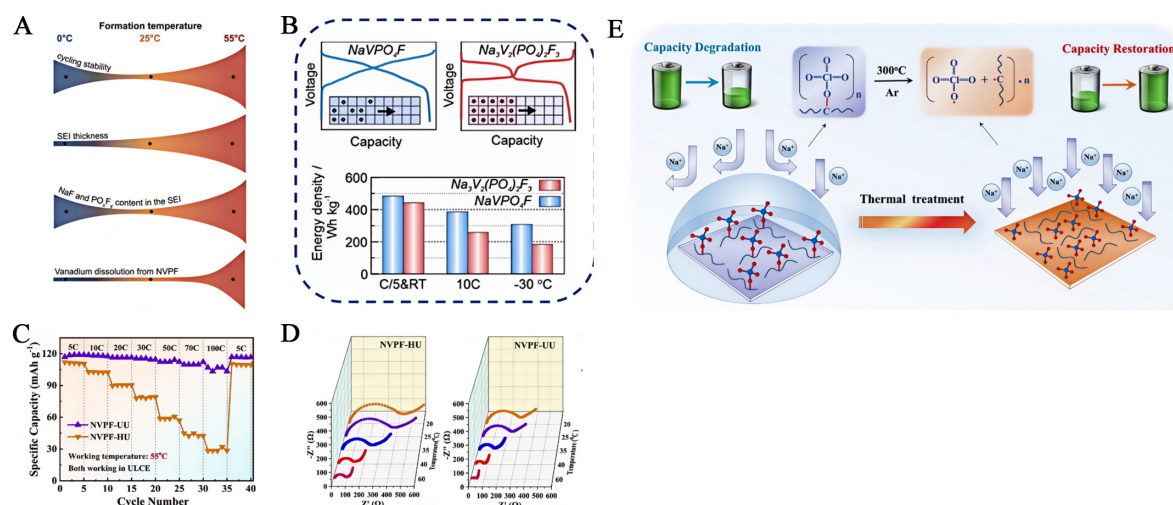


Figure 8. (A) Effect of temperature on different NVPF|HC cells parameters. Reproduced with permission^[196]. Copyright 2023, IOP Publishing; (B) Performance comparison at different temperatures. Reproduced with permission^[197]. Copyright 2023, American Chemical Society; (C) Rate capacity of the batteries; (D) Nyquist plots for NVPF-HU and NVPF-UU; (E) Effect of heat treatment on the failed NVPF-H cathode. Reproduced with permission^[200]. Copyright 2022, Wiley -VCH. NVPF|HC: Na₃V₂(PO₄)₂F₃|hard carbon.

C and -30 °C was 387 and 308 Wh kg⁻¹, respectively, compared with 259 and 184 Wh kg⁻¹ for NVPF. Although the Na⁺ diffusion coefficient in the single-phase region was similar for both materials, the decline in performance from the quasi-equilibrium charge-discharge state was caused by concentration polarization effects. In the case of NVPF, the slow movement of phase boundaries during phase transformation was the principal cause of the observed rapid capacity decay.

Molecular dynamics studies of the local nanostructure associated with a series of carbonate-based sodium electrolytes at the NVP and NVPF interfaces were conducted with an analysis of de-solvation^[198]. The results have indicated that the solvent filler behavior at the electrode surface is a key factor affecting the energy barrier height related to de-solvation. On a graphite electrode without SEI, no dissolution was observed due to the absence of specific oriented interactions between the solvent and the carbon sheet. However, in polyanion nested compounds with uneven surfaces and donor and acceptor groups, the closest layer of solvent molecules exhibited a distinct arrangement, with a partial loss of the Na⁺ solvation shell on passage through the layer. This effect was particularly pronounced on the NVP interface, and the high energy barrier was attributed to the highly ordered and well-oriented first solvent layer. The arrangement of the solvent was less pronounced at the NVPF interface due to the presence of non-polar fluorine atoms which interfered with the electrostatic attraction between the solvent and electrode.

Semykina *et al.*^[199] studied the mechanism and kinetics of the solid-phase reaction between NaF and VPO₄, along with the effect of high-energy ball-milling (HEBM). The results showed that the reaction proceeded in a “dimensionality reduction” manner, where the rate-limiting step involved the diffusion of Na⁺ and F⁻ through the single VPO₄ side. The macroscopic HEBM mechanism followed a third-order reaction model, enabling a significant increase in the rate constant and diffusion coefficient. The apparent activation energy was approximately 290 kJ mol⁻¹. The similarity in the structure of reactant (VPO₄) and product (NVPF) facilitated interaction with a partial occupation of Na⁺ sites that favored Na⁺ migration. The electrochemical performance of the prepared NVPF matched conventional materials.

An analysis of the interface between a high-voltage NVPF cathode and electrolyte in SIBs has revealed that the interface phase of high-concentration electrolytes was primarily composed of anions, including a significant presence of anion derivatives (C_xClO_y) and inorganic substances (Na_2CO_3 and NaF), which increased resistance to Na^+ transport and exacerbated gas evolution^[200]. In low-concentration electrolytes, the solvation structure of the contact ion pairs was conducive to forming a stable anion-regulated and solvent-derived composite interface phase, enhancing the cycling stability and the interfacial kinetic performance of the battery at 55 °C [Figure 8C and D]. In addition, the performance of the failed NVPF cathode could be restored by annealing [Figure 8E]. The C_xClO_y phase decomposed in argon at 300 °C, reconstructing the interface phase.

SUMMARY AND OUTLOOK

SIBs, exhibiting unique advantages with respect to the cost-effective supply of sodium and high-power density, are considered viable alternatives to LIBs. The use of NVPF with a NASICON structure as cathode material offers high operating potential and structural stability that has attracted significant research activity in SIB development and applications. This review has addressed the research progress made in the past three years regarding NVPF cathode materials for use in SIBs, examining synthesis methods, modification strategies, and component optimization. Despite significant advancements in NVPF development, numerous challenges lie ahead. We have summarized the technological progress and challenges [Figure 9], and anticipate the following future directions for the optimization of high-performance NVPF cathodes:

- (1) Synthesis of nano-structured NVPF can optimize Na^+ diffusion and enhance the interfacial contact between the active material and electrolyte. Existing studies of NVP morphology are insufficient, and there is an urgent need for a better understanding of the factors that control morphology. Furthermore, integrating multi-dimensional carbon materials to construct high-quality hierarchical carbon layers, forming abundant electron and ion transport pathways, represents a critical research direction. An exploration of other coating materials, such as Al_2O_3 and RuO_2 ^[201], can further develop effective composite synthesis strategies.
- (2) Current research on modification mechanisms is insufficient, particularly concerning theoretical models of NVPF crystal growth and an in-depth exploration of doping mechanisms. The chemical synergism associated with the crystalline NVPF positive electrode materials and the mechanism of valence changes may be revealed by utilizing advanced characterization techniques, such as solid-state nuclear magnetic resonance, X-ray absorption spectroscopy, and combining these measurements with first-principles calculations based on DFT^[194].
- (3) It is particularly important to develop effective Na^+ compensation methods to address the issue of reduced energy density due to Na loss. Introducing suitable additives to NVPF or the electrolyte represents a feasible approach. It is crucial to thoroughly investigate the effects of electrolyte formulations, concentrations, and types of additives, focusing on such parameters as coulomb efficiency, cycle life, and rate performance^[182]. It is essential to develop electrolytes that are stable over a wider temperature range in order to satisfy the requirements of practical application^[202]. The research and development of solid-state electrolytes represent a potential means of enhancing the electrochemical performance of NVPF-based batteries at high temperatures.
- (4) The role of binders must be considered, with systematic testing in order to screen and identify the most suitable binder. This must include an assessment of the physical and chemical properties of the binder in relation to NVPF, and the associated impact on performance^[194]. In addition, the production of structures



Figure 9. The progress in technology and future challenges of NVPF in SIBs. NVPF: $\text{Na}_3\text{V}_2(\text{PO}_4)_2\text{F}_3$; SIB: sodium-ion battery; SEI: solid electrolyte interphase; CEI: cathode-electrolyte interface.

without the need for binders should be examined.

This review has offered new insights into the synthesis and design of high-performance NVPF cathode materials. Given the rapid progress of SIB technology, we anticipate the emergence of a series of NVPF cathode materials with superior electrochemical properties in the near future, paving the way for commercial applications.

DECLARATIONS

Acknowledgments

We thank EditSprings (<https://www.editsprings.cn>) for the expert linguistic assistance during the preparation of this manuscript.

Authors' contributions

Conceptualization: Liang, Y.; Chen, Z.; Sun, Z.
 Writing-original draft: Liang, Y.
 Writing of review and editing: Chen, Z, Sun, Z.
 Supervision: Ning, D.; Chen, Z.; Sun, Z.
 Project administration: Xu, L.; Chen, Z.; Sun, Z.

Availability of data and materials

Not applicable.

Financial support and sponsorship

The authors acknowledge the National Natural Science Foundation of China (Nos. 52202304, 22473032), Guangdong Province Science and Technology Plan Project (Nos. 2024B1212050006, 2022A0505020010), Guangdong Provincial University Key Project (No. 2022ZDZX3043), Zhuhai Innovation and Entrepreneurship Team Project (No. 22055905200017), Zhuhai Science and Technology Department Project (Nos. 2420004000114, 2420004000003, 2320004000233), Guangdong University of Technology Hundred Talents Program (No. 263118136), and Marine Biomaterials Laboratory of ZIAT and Dangan Town.

Conflicts of interest

All authors declared that there are no conflicts of interest.

Ethical approval and consent to participate

Not applicable.

Consent for publication

Not applicable.

Copyright

© The Author(s) 2025.

REFERENCES

1. Obama, B. The irreversible momentum of clean energy. *Science* **2017**, 355, 126-9. DOI PubMed
2. Deng, X.; Li, J.; Ma, L.; Sha, J.; Zhao, N. Three-dimensional porous carbon materials and their composites as electrodes for electrochemical energy storage systems. *Mater. Chem. Front.* **2019**, 3, 2221-45. DOI
3. Zeng, X.; Xu, Y.; Yin, Y.; Wu, X.; Yue, J.; Guo, Y. Recent advances in nanostructured electrode-electrolyte design for safe and next-generation electrochemical energy storage. *Mater. Today. Nano.* **2019**, 8, 100057. DOI
4. Liu, X.; Wang, Y.; Yang, Y.; et al. A MoS₂/Carbon hybrid anode for high-performance Li-ion batteries at low temperature. *Nano. Energy.* **2020**, 70, 104550. DOI
5. Usiskin, R.; Lu, Y.; Popovic, J.; et al. Fundamentals, status and promise of sodium-based batteries. *Nat. Rev. Mater.* **2021**, 6, 1020-35. DOI
6. Perveen, T.; Siddiq, M.; Shahzad, N.; Ihsan, R.; Ahmad, A.; Shahzad, M. I. Prospects in anode materials for sodium ion batteries - a review. *Renew. Sust. Energ. Rev.* **2020**, 119, 109549. DOI
7. Fan, E.; Li, L.; Wang, Z.; et al. Sustainable recycling technology for Li-Ion batteries and beyond: challenges and future prospects. *Chem. Rev.* **2020**, 120, 7020-63. DOI
8. Jiao, J.; Wu, K.; Li, N.; et al. Tuning anionic redox activity to boost high-performance sodium-storage in low-cost Na_{0.67}Fe_{0.5}Mn_{0.5}O₂ cathode. *J. Energy. Chem.* **2022**, 73, 214-22. DOI
9. Qi, Y.; Tong, Z.; Zhao, J.; et al. Scalable room-temperature synthesis of multi-shelled Na₃(VOPO₄)₂F microsphere cathodes. *Joule* **2018**, 2, 2348-63. DOI
10. Hwang, J. Y.; Myung, S. T.; Sun, Y. K. Sodium-ion batteries: present and future. *Chem. Soc. Rev.* **2017**, 46, 3529-614. DOI PubMed
11. Rajagopalan, R.; Tang, Y.; Jia, C.; Ji, X.; Wang, H. Understanding the sodium storage mechanisms of organic electrodes in sodium ion batteries: issues and solutions. *Energy. Environ. Sci.* **2020**, 13, 1568-92. DOI
12. Xie, F.; Chen, J.; Xu, J.; et al. Investigation of Na₃V₃(P₂O₇)₄/carbon composite as cathode material for sodium-ion battery: influences of carbon additives and voltage windows. *J. Energy. Storage.* **2024**, 77, 109855. DOI
13. Fang, Y.; Zhang, J.; Xiao, L.; Ai, X.; Cao, Y.; Yang, H. Phosphate framework electrode materials for sodium ion batteries. *Adv. Sci. (Weinh).* **2017**, 4, 1600392. DOI PubMed PMC
14. Chen, S.; Wu, C.; Shen, L.; et al. Challenges and perspectives for NASICON-type electrode materials for advanced sodium-ion batteries. *Adv. Mater.* **2017**, 29. DOI
15. Zhuang, S.; Yang, C.; Zheng, M.; et al. A combined first principles and experimental study on Al-doped Na₃V₂(PO₄)₂F₃ cathode for rechargeable Na batteries. *Surf. Coat. Tech.* **2022**, 434, 128184. DOI

16. Zhou, L.; Zhuang, Z.; Zhao, H.; Lin, M.; Zhao, D.; Mai, L. Intricate hollow structures: controlled synthesis and applications in energy storage and conversion. *Adv. Mater.* **2017**, *29*. DOI
17. Sun, D.; Ye, D.; Liu, P.; et al. MoS₂/graphene nanosheets from commercial bulky MoS₂ and graphite as anode materials for high rate sodium-ion batteries. *Adv. Energy Mater.* **2018**, *8*, 1702383. DOI
18. Wang, W.; Li, W.; Wang, S.; Miao, Z.; Liu, H. K.; Chou, S. Structural design of anode materials for sodium-ion batteries. *J. Mater. Chem. A* **2018**, *6*, 6183-205. DOI
19. Xue, X.; Sun, D.; Zeng, X.; et al. Two-step carbon modification of NaTi₂(PO₄)₃ with improved sodium storage performance for Na-ion batteries. *J. Cent. South. Univ.* **2018**, *25*, 2320-31. DOI
20. Huang, Z.; Hou, H.; Wang, C.; Li, S.; Zhang, Y.; Ji, X. Molybdenum phosphide: a conversion-type anode for ultralong-life sodium-ion batteries. *Chem. Mater.* **2017**, *29*, 7313-22. DOI
21. Sun, D.; Luo, B.; Wang, H.; Tang, Y.; Ji, X.; Wang, L. Engineering the trap effect of residual oxygen atoms and defects in hard carbon anode towards high initial Coulombic efficiency. *Nano. Energy* **2019**, *64*, 103937. DOI
22. Liu, N.; He, Z.; Zhu, J.; et al. Crystal doping of K ion on Na site raises the electrochemical performance of NaTi₂(PO₄)₃/C anode for sodium-ion battery. *Ionics* **2020**, *26*, 3387-94. DOI
23. Lao, M.; Zhang, Y.; Luo, W.; Yan, Q.; Sun, W.; Dou, S. X. Alloy-based anode materials toward advanced sodium-ion batteries. *Adv. Mater.* **2017**, *29*. DOI
24. Hao, Y.; Li, X.; Liu, W.; et al. Depolarization of Li-rich Mn-based oxide via electrochemically active Prussian blue interface providing superior rate capability. *Carbon. Energy* **2023**, *5*, e272. DOI
25. Su, H.; Jaffer, S.; Yu, H. Transition metal oxides for sodium-ion batteries. *Energy. Storage. Mater.* **2016**, *5*, 116-31. DOI
26. Cao, Y.; He, Y.; Gang, H.; et al. Stability study of transition metal oxide electrode materials. *J. Power. Sources* **2023**, *560*, 232710. DOI
27. Sang, L.; Wang, K.; Wu, Y.; Ma, C. The improved solar weighted absorptance and thermal stability of desert sand coated with transition metal oxides for direct particle receiver. *Sol. Energy. Mater. Sol. Cells* **2023**, *251*, 112158. DOI
28. Rao, T.; Zhou, Y.; Jiang, J.; Yang, P.; Liao, W. Low dimensional transition metal oxide towards advanced electrochromic devices. *Nano. Energy* **2022**, *100*, 107479. DOI
29. Liu, Z.; Huang, Y.; Huang, Y.; et al. Voltage issue of aqueous rechargeable metal-ion batteries. *Chem. Soc. Rev.* **2020**, *49*, 180-232. DOI PubMed
30. Camacho, P. S.; Wernert, R.; Duttine, M.; et al. Impact of synthesis conditions in Na-rich Prussian blue analogues. *ACS. Appl. Mater. Interfaces* **2021**, *13*, 42682-92. DOI
31. Li, J.; Yi, H.; Xiao, Y.; et al. Freestanding catalytic membranes assembled from blade-shaped Prussian blue analog sheets for flow-through degradation of antibiotic pollutants. *Appl. Catal. B: Environ.* **2023**, *336*, 122922. DOI
32. Chun, J.; Wang, X.; Wei, C.; Wang, Z.; Zhang, Y.; Feng, J. Flexible and free-supporting Prussian blue analogs /MXene film for high-performance sodium-ion batteries. *J. Power. Sources* **2023**, *576*, 233165. DOI
33. Han, J.; Hu, Y.; Han, Q.; Liu, X.; Wang, C. Synthesis of high-specific-capacity Prussian blue analogues for sodium-ion batteries boosted by grooved structure. *J. Alloys. Compd.* **2023**, *950*, 169928. DOI
34. Xu, N.; Lei, H.; Hou, T.; et al. Constructing an asymmetric supercapacitor based on Prussian blue analogues-derived cobalt selenide nanoframeworks and iron oxide nanoparticles. *Electrochimica. Acta* **2023**, *439*, 141686. DOI
35. Yang, Y.; Guo, C.; Zeng, Y.; Luo, Y.; Xu, J.; Wang, C. Peroxymonosulfate activation by CuFe-Prussian blue analogues for the degradation of bisphenol S: effect, mechanism, and pathway. *Chemosphere* **2023**, *331*, 138748. DOI
36. Okubo, M.; Li, C. H.; Talham, D. R. High rate sodium ion insertion into core-shell nanoparticles of Prussian blue analogues. *Chem. Commun. (Camb)* **2014**, *50*, 1353-5. DOI PubMed
37. He, M.; Davis, R.; Chartouni, D.; et al. Assessment of the first commercial Prussian blue based sodium-ion battery. *J. Power. Sources* **2022**, *548*, 232036. DOI
38. Yue, Y.; Binder, A. J.; Guo, B.; et al. Mesoporous Prussian blue analogues: template-free synthesis and sodium-ion battery applications. *Angew. Chem. Int. Ed. Engl.* **2014**, *53*, 3134-7. DOI
39. Peng, J.; Zhang, W.; Liu, Q.; et al. Prussian blue analogues for sodium-ion batteries: past, present, and future. *Adv. Mater.* **2022**, *34*, e2108384. DOI
40. Wang, W.; Gang, Y.; Hu, Z.; et al. Reversible structural evolution of sodium-rich rhombohedral Prussian blue for sodium-ion batteries. *Nat. Commun.* **2020**, *11*, 980. DOI PubMed PMC
41. Dong, Y.; Di, S.; Zhang, F.; et al. Nonaqueous electrolyte with dual-cations for high-voltage and long-life zinc batteries. *J. Mater. Chem. A* **2020**, *8*, 3252-61. DOI
42. Ni, Q.; Bai, Y.; Wu, F.; Wu, C. Polyanion-type electrode materials for sodium-ion batteries. *Adv. Sci. (Weinh)* **2017**, *4*, 1600275. DOI PubMed PMC
43. Zhao, L.; Zhang, T.; Zhao, H.; Hou, Y. Polyanion-type electrode materials for advanced sodium-ion batteries. *Mater. Today. Nano* **2020**, *10*, 100072. DOI
44. Yuan, Y.; Wei, Q.; Yang, S.; et al. Towards high-performance phosphate-based polyanion-type materials for sodium-ion batteries. *Energy. Storage. Mater.* **2022**, *50*, 760-82. DOI
45. Gao, Y.; Zhang, H.; Liu, X.; et al. Low-cost polyanion-type sulfate cathode for sodium-ion battery. *Adv. Energy. Mater.* **2021**, *11*, 2101751. DOI

46. Yuan, D.; Liang, X.; Wu, L.; et al. A honeycomb-layered $\text{Na}_3\text{Ni}_2\text{SbO}_6$: a high-rate and cycle-stable cathode for sodium-ion batteries. *Adv. Mater.* **2014**, 26, 6301-6. DOI
47. You, Y.; Wu, X.; Yin, Y.; Guo, Y. High-quality Prussian blue crystals as superior cathode materials for room-temperature sodium-ion batteries. *Energy. Environ. Sci.* **2014**, 7, 1643-7. DOI
48. Wang, L.; Song, J.; Qiao, R.; et al. Rhombohedral Prussian white as cathode for rechargeable sodium-ion batteries. *J. Am. Chem. Soc.* **2015**, 137, 2548-54. DOI
49. Jin, T.; Li, H.; Zhu, K.; Wang, P. F.; Liu, P.; Jiao, L. Polyanion-type cathode materials for sodium-ion batteries. *Chem. Soc. Rev.* **2020**, 49, 2342-77. DOI
50. Xiang, X.; Zhang, K.; Chen, J. Recent advances and prospects of cathode materials for sodium-ion batteries. *Adv. Mater.* **2015**, 27, 5343-64. DOI
51. Liang, K.; Wu, D.; Ren, Y.; Huang, X.; Ma, J. Research progress on $\text{Na}_3\text{V}_2(\text{PO}_4)_2\text{F}_3$ -based cathode materials for sodium-ion batteries. *Chin. Chem. Lett.* **2023**, 34, 107978. DOI
52. Rajagopalan, R.; Tang, Y.; Ji, X.; Jia, C.; Wang, H. Advancements and challenges in potassium ion batteries: a comprehensive review. *Adv. Funct. Mater.* **2020**, 30, 1909486. DOI
53. Chen, Y.; Zhao, Y.; Tian, S.; Wang, P.; Qiu, F.; Yi, T. Recent progress and strategic perspectives of high-voltage $\text{Na}_3\text{V}_2(\text{PO}_4)_2\text{F}_3$ cathode: fundamentals, modifications, and applications in sodium-ion batteries. *Compos. B.: Eng.* **2023**, 266, 111030. DOI
54. Hu, J.; Zhao, W.; Wang, Y.; et al. The role of fluorine in polyanionic cathode materials for sodium-ion batteries. *Small. Methods.* **2025**, e2402099. DOI
55. Zhu, L.; Wang, H.; Sun, D.; Tang, Y.; Wang, H. A comprehensive review on the fabrication, modification and applications of $\text{Na}_3\text{V}_2(\text{PO}_4)_2\text{F}_3$ cathodes. *J. Mater. Chem. A.* **2020**, 8, 21387-407. DOI
56. Bianchini, M.; Brisset, N.; Fauth, F.; et al. $\text{Na}_3\text{V}_2(\text{PO}_4)_2\text{F}_3$ revisited: a high-resolution diffraction study. *Chem. Mater.* **2014**, 26, 4238-47. DOI
57. Bianchini, M.; Fauth, F.; Brisset, N.; et al. Comprehensive investigation of the $\text{Na}_3\text{V}_2(\text{PO}_4)_2\text{F}_3$ - $\text{Na}_3\text{V}_2(\text{PO}_4)_2\text{F}_3$ system by operando high resolution synchrotron X-ray diffraction. *Chem. Mater.* **2015**, 27, 3009-20. DOI
58. Chen, X.; Wu, Q.; Guo, P.; Liu, X. Rational design of two dimensional single crystalline $\text{Na}_3\text{V}_2(\text{PO}_4)_2\text{F}_3$ nanosheets for boosting Na^+ migration and mitigating grain pulverization. *J. Chem. Eng.* **2022**, 439, 135533. DOI
59. Deng, L.; Yu, F.; Xia, Y.; et al. Stabilizing fluorine to achieve high-voltage and ultra-stable $\text{Na}_3\text{V}_2(\text{PO}_4)_2\text{F}_3$ cathode for sodium ion batteries. *Nano. Energy.* **2021**, 82, 105659. DOI
60. Gu, Z. Y.; Guo, J. Z.; Cao, J. M.; et al. An advanced high-entropy fluorophosphate cathode for sodium-ion batteries with increased working voltage and energy density. *Adv. Mater.* **2022**, 34, e2110108. DOI
61. Li, L.; Zhang, N.; Su, Y.; et al. Fluorine dissolution-induced capacity degradation for fluorophosphate-based cathode materials. *ACS. Appl. Mater. Interfaces.* **2021**, 13, 23787-93. DOI
62. Yang, Z.; Li, G.; Sun, J.; et al. High performance cathode material based on $\text{Na}_3\text{V}_2(\text{PO}_4)_2\text{F}_3$ and $\text{Na}_3\text{V}_2(\text{PO}_4)_2\text{F}_3$ for sodium-ion batteries. *Energy. Storage. Mater.* **2020**, 25, 724-30. DOI
63. Yi, H.; Ling, M.; Xu, W.; Li, X.; Zheng, Q.; Zhang, H. VSC-doping and VSU-doping of $\text{Na}_3\text{V}_{2-x}\text{Ti}_x(\text{PO}_4)_2\text{F}_3$ compounds for sodium ion battery cathodes: analysis of electrochemical performance and kinetic properties. *Nano. Energy.* **2018**, 47, 340-52. DOI
64. Deng, L.; Sun, G.; Goh, K.; et al. Facile one-step carbothermal reduction synthesis of $\text{Na}_3\text{V}_2(\text{PO}_4)_2\text{F}_3/\text{C}$ serving as cathode for sodium ion batteries. *Electrochimica. Acta.* **2019**, 298, 459-67. DOI
65. Zhang, B.; Dugas, R.; Rousse, G.; Rozier, P.; Abakumov, A. M.; Tarascon, J. M. Insertion compounds and composites made by ball milling for advanced sodium-ion batteries. *Nat. Commun.* **2016**, 7, 10308. DOI PubMed PMC
66. Wang, M.; Huang, X.; Wang, H.; Zhou, T.; Xie, H.; Ren, Y. Synthesis and electrochemical performances of $\text{Na}_3\text{V}_2(\text{PO}_4)_2\text{F}_3/\text{C}$ composites as cathode materials for sodium ion batteries. *RSC. Adv.* **2019**, 9, 30628-36. DOI PubMed PMC
67. Liu, Q.; Wang, D.; Yang, X.; et al. Carbon-coated $\text{Na}_3\text{V}_2(\text{PO}_4)_2\text{F}_3$ nanoparticles embedded in a mesoporous carbon matrix as a potential cathode material for sodium-ion batteries with superior rate capability and long-term cycle life. *J. Mater. Chem. A.* **2015**, 3, 21478-85. DOI
68. Li, L.; Xu, Y.; Sun, X.; He, S.; Li, L. High capacity-favorable tap density cathode material based on three-dimensional carbonous framework supported $\text{Na}_3\text{V}_2(\text{PO}_4)_2\text{F}_3$ nanoparticles. *Chem. Eng. J.* **2018**, 331, 712-9. DOI
69. Liu, Q.; Meng, X.; Wei, Z.; et al. Core/Double-shell structured $\text{Na}_3\text{V}_2(\text{PO}_4)_2\text{F}_3@\text{C}$ nanocomposite as the high power and long lifespan cathode for sodium-ion batteries. *ACS. Appl. Mater. Interfaces.* **2016**, 8, 31709-15. DOI
70. Jiang, T.; Chen, G.; Li, A.; Wang, C.; Wei, Y. Sol-gel preparation and electrochemical properties of $\text{Na}_3\text{V}_2(\text{PO}_4)_2\text{F}_3/\text{C}$ composite cathode material for lithium ion batteries. *J. Alloys. Compd.* **2009**, 478, 604-7. DOI
71. Eshraghi, N.; Caes, S.; Mahmoud, A.; Cloots, R.; Vertruyen, B.; Boschini, F. Sodium vanadium (III) fluorophosphate/carbon nanotubes composite (NVPF/CNT) prepared by spray-drying: good electrochemical performance thanks to well-dispersed CNT network within NVPF particles. *Electrochimica. Acta.* **2017**, 228, 319-24. DOI
72. Shen, C.; Long, H.; Wang, G.; Lu, W.; Shao, L.; Xie, K. $\text{Na}_3\text{V}_2(\text{PO}_4)_2\text{F}_3@\text{C}$ dispersed within carbon nanotube frameworks as a high tap density cathode for high-performance sodium-ion batteries. *J. Mater. Chem. A.* **2018**, 6, 6007-14. DOI
73. Leng, J.; Wang, Z.; Wang, J.; et al. Advances in nanostructures fabricated via spray pyrolysis and their applications in energy storage and conversion. *Chem. Soc. Rev.* **2019**, 48, 3015-72. DOI
74. Yi, H.; Lin, L.; Ling, M.; et al. Scalable and economic synthesis of high-performance $\text{Na}_3\text{V}_2(\text{PO}_4)_2\text{F}_3$ by a solvothermal-ball-milling

- method. *ACS. Energy. Lett.* **2019**, *4*, 1565-71. DOI
75. Hu, F.; Jiang, X. Superior performance of carbon modified $\text{Na}_3\text{V}_2(\text{PO}_4)_2\text{F}_3$ cathode material for sodium-ion batteries. *Inorg. Chem. Commun.* **2021**, *129*, 108653. DOI
76. Cai, Y.; Cao, X.; Luo, Z.; et al. Caging $\text{Na}_3\text{V}_2(\text{PO}_4)_2\text{F}_3$ microcubes in cross-linked graphene enabling ultrafast sodium storage and long-term cycling. *Adv. Sci. (Weinh)*. **2018**, *5*, 1800680. DOI PubMed PMC
77. Li, Y.; Liang, X.; Zhong, G.; et al. Fiber-shape $\text{Na}_3\text{V}_2(\text{PO}_4)_2\text{F}_3$ @N-Doped carbon as a cathode material with enhanced cycling stability for Na-ion batteries. *ACS. Appl. Mater. Interfaces*. **2020**, *12*, 25920-9. DOI
78. Li, X.; Chen, W.; Qian, Q.; et al. Electrospinning-based strategies for battery materials. *Adv. Energy. Mater.* **2021**, *11*, 2000845. DOI
79. Qiu, R.; Fei, R.; Guo, J.; et al. Encapsulation of $\text{Na}_3(\text{VO})_2(\text{PO}_4)_2\text{F}$ into carbon nanofiber as an superior cathode material for flexible sodium-ion capacitors with high-energy-density and low-self-discharge. *J. Power. Sources*. **2020**, *466*, 228249. DOI
80. Shen, X.; Zhou, Q.; Han, M.; et al. Rapid mechanochemical synthesis of polyanionic cathode with improved electrochemical performance for Na-ion batteries. *Nat. Commun.* **2021**, *12*, 2848. DOI PubMed PMC
81. Minart, G.; Croguennec, L.; Weill, F.; Labrugère-Sarroste, C.; Olchowka, J. Increasing tap density of carbon-coated $\text{Na}_3\text{V}_2(\text{PO}_4)_2\text{F}_3$ via mechanical grinding: good or bad idea? *ACS. Appl. Energy. Mater.* **2024**, *7*, 11334-42. DOI
82. Serras, P.; Palomares, V.; Goñi, A.; Kubiak, P.; Rojo, T. Electrochemical performance of mixed valence $\text{Na}_3\text{V}_2\text{O}_{2x}(\text{PO}_4)_2\text{F}_{3-2x}/\text{C}$ as cathode for sodium-ion batteries. *J. Power. Sources*. **2013**, *241*, 56-60. DOI
83. Serras, P.; Palomares, V.; Goñi, A.; et al. High voltage cathode materials for Na-ion batteries of general formula $\text{Na}_3\text{V}_2\text{O}_{2x}(\text{PO}_4)_2\text{F}_{3-2x}$. *J. Mater. Chem.* **2012**, *22*, 22301. DOI
84. Zhu, P.; Peng, W.; Guo, H.; et al. Toward high-performance sodium storage cathode: construction and purification of carbon-coated $\text{Na}_3\text{V}_2(\text{PO}_4)_2\text{F}_3$ materials. *J. Power. Sources*. **2022**, *546*, 231986. DOI
85. Jiang, N.; Zhang, L.; Cui, C.; Gao, L.; Yang, X. Synthesis and electrochemical performance of uniform carbon-coated $\text{Na}_3\text{V}_2(\text{PO}_4)_2\text{F}_3$ using tannic acid as a chelating agent and carbon source. *ACS. Appl. Energy. Mater.* **2022**, *5*, 249-56. DOI
86. Zhang, J.; Zhang, C.; Han, Y.; Zhao, X.; Liu, W.; Ding, Y. A surface-modified $\text{Na}_3\text{V}_2(\text{PO}_4)_2\text{F}_3$ cathode with high rate capability and cycling stability for sodium ion batteries. *RSC. Adv.* **2024**, *14*, 13703-10. DOI PubMed PMC
87. Wang, S.; Li, J.; Xu, L.; et al. Manipulation of $\text{Na}_3\text{V}_2(\text{PO}_4)_2\text{F}_3$ via aluminum doping to alter local electron states toward an advanced cathode for sodium-ion batteries. *Rare. Met.* **2024**, *43*, 4253-62. DOI
88. Guan, J.; Zhou, S.; Zhou, J.; et al. Microwave-assisted hydrothermal synthesis of $\text{Na}_3\text{V}_2(\text{PO}_4)_2\text{F}_3$ nanocuboid@reduced graphene oxide as an ultrahigh-rate and superlong-lifespan cathode for fast-charging sodium-ion batteries. *ACS. Appl. Mater. Interfaces*. **2024**, DOI
89. Al-Marri, A. H. Superior electrochemical properties of $\text{Na}_3\text{V}_2(\text{PO}_4)_2\text{F}_3/\text{rGO}$ composite cathode for high-performance sodium-ion batteries. *J. Solid. State. Electrochem.* **2024**, *28*, 2861-72. DOI
90. Liang, K.; Zhao, H.; Li, J.; et al. Engineering crystal growth and surface modification of $\text{Na}_3\text{V}_2(\text{PO}_4)_2\text{F}_3$ cathode for high-energy-density sodium-ion batteries. *Small* **2023**, *19*, e2207562. DOI
91. Zhai, X.; Chen, X.; Zhang, Q.; et al. Temperature-dependent defect evolution and electrochemical performance enhancement of $\text{Na}_3\text{V}_2(\text{PO}_4)_2\text{F}_3$. *J. Alloys. Compd.* **2023**, *952*, 170001. DOI
92. Lin, Z. Phase formation in $\text{NaH}_2\text{PO}_4\text{-VOSO}_4\text{-NaF-H}_2\text{O}$ system and rapid synthesis of $\text{Na}_3\text{V}_2\text{O}_{2x}(\text{PO}_4)_2\text{F}_{3-2x}$. *Crystals* **2024**, *14*, 43. DOI
93. Wang, S.; Liang, K.; Li, J.; Huang, X.; Ren, Y. Surfactant-assisted synthesis of self-assembled $\text{Na}_3\text{V}_2(\text{PO}_4)_2\text{F}_3$ @C microspheres as the cathode for Na-ion batteries. *Vacuum* **2023**, *211*, 111894. DOI
94. Moossa, B.; Abraham, J. J.; Ahmed, A. M.; Kahraman, R.; Al-qaradawi, S.; Shakoor, R. Synergistic effect of NASICON $\text{Na}_3\text{V}_2(\text{PO}_4)_2\text{F}_3$ and 2D MXene for high-performance symmetric Sodium-ion batteries. *Mater. Res. Bull.* **2025**, *182*, 113173. DOI
95. Guo, S.; Peng, J.; Sharma, N.; et al. Optimizing Sc-doped $\text{Na}_3\text{V}_2(\text{PO}_4)_2\text{F}_3/\text{C}$ as a high-performance cathode material for sodium-ion battery applications. *Chem. Mater.* **2025**, *37*, 1500-12. DOI
96. Sun, C.; Zhang, L.; Xiong, X.; Deng, Z.; Sun, H.; Yang, X. Electronic/Ionic dual functional layer-coated $\text{Na}_3\text{V}_2(\text{PO}_4)_2\text{F}_3$ cathode with high sodium storage performance. *ACS. Sustainable. Chem. Eng.* **2024**, *12*, 10892-904. DOI
97. Yang, Y.; Xu, G. R.; Tang, A. P.; et al. $\text{Na}_3\text{V}_2(\text{PO}_4)_2\text{F}_3$ -decorated $\text{Na}_3\text{V}_2(\text{PO}_4)_2\text{F}_3$ as a high-rate and cycle-stable cathode material for sodium ion batteries. *RSC. Adv.* **2024**, *14*, 11862-71. DOI
98. Qin, Y.; Li, L.; Zhao, H.; et al. Effect of chelator content on the structural and electrochemical performance of $\text{Na}_3\text{V}_2(\text{PO}_4)_2\text{F}_3$ by sol-gel preparation. *CrystEngComm* **2022**, *24*, 4519-26. DOI
99. Mahato, S.; Das, S.; Gupta, D.; Biswas, K. Vanadium substituted Fe, Cr co-doped high performance $\text{C}/\text{Na}_3\text{V}_2(\text{PO}_4)_2\text{F}_3$ cathode for sodium-ion batteries. *J. Electroanal. Chem.* **2024**, *955*, 118046. DOI
100. Liang, K.; Zhao, H.; Li, J.; Huang, X.; Ren, Y. High-performance $\text{Na}_3\text{V}_2(\text{PO}_4)_2\text{F}_3$ cathode obtained by a three-in-one strategy for self-sodium compensation, interface modification, and crosslinked carbon coatings. *Appl. Surface. Sci.* **2023**, *615*, 156412. DOI
101. Hu, Z.; Zhang, R.; Fan, C.; et al. Synergistic effect, structural and morphology evolution, and doping mechanism of spherical Br-doped $\text{Na}_3\text{V}_2(\text{PO}_4)_2\text{F}_3/\text{C}$ toward enhanced sodium storage. *Small* **2022**, *18*, e2201719. DOI
102. Zhou, Q.; Wang, Y.; Ou, R.; et al. Yolk-Shell Construction of $\text{Na}_3\text{V}_2(\text{PO}_4)_2\text{F}_3$ with copper substitution microsphere as high-rate and long-cycling cathode materials for sodium-ion batteries. *Small* **2024**, *20*, e2310699. DOI
103. Lei, L.; Sun, K.; Zhao, H.; Wang, C.; Wei, T. Large scale preparation of $\text{Na}_3\text{V}_2(\text{PO}_4)_2\text{F}_3$ with cross-linked double carbon network for high energy density sodium ion batteries at -20 °C. *J. Energy. Storage*. **2024**, *78*, 109923. DOI

104. Guo, R.; Li, W.; Lu, M.; et al. $\text{Na}_3\text{V}_2(\text{PO}_4)_2\text{F}_3$ @bagasse carbon as cathode material for lithium/sodium hybrid ion battery. *Phys. Chem. Chem. Phys.* **2022**, 24, 5638-45. DOI
105. Liang, M.; Li, W.; Yang, Y.; et al. Carbon Nanofiber/ $\text{Na}_3\text{V}_2(\text{PO}_4)_2\text{F}_3$ particle composites as a self-standing cathode for high-voltage flexible sodium-ion batteries. *ACS. Appl. Nano. Mater.* **2023**, 6, 22275-82. DOI
106. Song, Z.; Liu, Y.; Guo, Z.; et al. Ultrafast synthesis of large-sized and conductive $\text{Na}_3\text{V}_2(\text{PO}_4)_2\text{F}_3$ simultaneously approaches high tap density, rate and cycling capability. *Adv. Funct. Mater.* **2024**, 34, 2313998. DOI
107. Wang, J.; Jing, H.; Wang, X.; et al. Electrostatically shielded transportation enabling accelerated Na^+ diffusivity in high-performance fluorophosphate cathode for sodium-ion batteries. *Adv. Funct. Mater.* **2024**, 34, 2315318. DOI
108. Ling, R.; Zhao, S.; Yang, C.; Qi, W. Three-dimensional ordered microporous $\text{Na}_3\text{V}_2(\text{PO}_4)_2\text{F}_3$ @C/carbon cloth as high-rate and stable flexible cathodes for Na-ion and Zn-ion batteries. *Appl. Surf. Sci.* **2023**, 620, 156875. DOI
109. Gu, Z. Y.; Guo, J. Z.; Sun, Z. H.; et al. Carbon-coating-increased working voltage and energy density towards an advanced $\text{Na}_3\text{V}_2(\text{PO}_4)_2\text{F}_3$ @C cathode in sodium-ion batteries. *Sci. Bull. (Beijing)*. **2020**, 65, 702-10. DOI
110. Zhang, L. L.; Zhou, Y. X.; Li, T.; Ma, D.; Yang, X. L. Multi-heteroatom doped carbon coated $\text{Na}_3\text{V}_2(\text{PO}_4)_2\text{F}_3$ derived from ionic liquids. *Dalton. Trans.* **2018**, 47, 4259-66. DOI
111. Li, F.; Zhao, Y.; Xia, L.; Yang, Z.; Wei, J.; Zhou, Z. Well-dispersed $\text{Na}_3\text{V}_2(\text{PO}_4)_2\text{F}_3$ @rGO with improved kinetics for high-power sodium-ion batteries. *J. Mater. Chem. A*. **2020**, 8, 12391-7. DOI
112. Yang, X.; Wang, X.; Zhen, W. Reversible Na^+ -extraction/insertion in nitrogen-doped graphene-encapsulated $\text{Na}_3\text{V}_2(\text{PO}_4)_2\text{F}_3$ @C electrode for advanced Na-ion battery. *Ceram. Int.* **2020**, 46, 9170-5. DOI
113. Hu, L.; Cheng, S.; Xiao, S.; et al. Dually decorated $\text{Na}_3\text{V}_2(\text{PO}_4)_2\text{F}_3$ by carbon and 3D graphene as cathode material for sodium-ion batteries with high energy and power densities. *ChemElectroChem* **2020**, 7, 3975-83. DOI
114. Guo, H.; Hu, Y.; Zhang, X.; et al. Facile one-step hydrothermal synthesis of $\text{Na}_3\text{V}_2(\text{PO}_4)_2\text{F}_3$ /CNTs tetragonal micro-particles as high performance cathode material for Na-ion batteries. *Front. Chem.* **2019**, 7, 689. DOI PubMed PMC
115. Kosova, N.; Rezepova, D. Mixed sodium-lithium vanadium fluorophosphates $\text{Na}_{3-x}\text{Li}_x\text{V}_2(\text{PO}_4)_2\text{F}_3$: the origin of the excellent high-rate performance. *J. Power. Sources*. **2018**, 408, 120-7. DOI
116. Li, L.; Liu, X.; Tang, L.; Liu, H.; Wang, Y. Improved electrochemical performance of high voltage cathode $\text{Na}_3\text{V}_2(\text{PO}_4)_2\text{F}_3$ for Na-ion batteries through potassium doping. *J. Alloys. Compd.* **2019**, 790, 203-11. DOI
117. Liu, W.; Yi, H.; Zheng, Q.; Li, X.; Zhang, H. Y-doped $\text{Na}_3\text{V}_2(\text{PO}_4)_2\text{F}_3$ compounds for sodium ion battery cathodes: electrochemical performance and analysis of kinetic properties. *J. Mater. Chem. A*. **2017**, 5, 10928-35. DOI
118. Criado, A.; Lavela, P.; Pérez-vicente, C.; Ortiz, G.; Tirado, J. Effect of chromium doping on $\text{Na}_3\text{V}_2(\text{PO}_4)_2\text{F}_3$ @C as promising positive electrode for sodium-ion batteries. *J. Electroanal. Chem.* **2020**, 856, 113694. DOI
119. Guo, C.; Yang, J.; Cui, Z.; et al. *In-situ* structural evolution analysis of Zr-doped $\text{Na}_3\text{V}_2(\text{PO}_4)_2\text{F}_3$ coated by N-doped carbon layer as high-performance cathode for sodium-ion batteries. *J. Energy. Chem.* **2022**, 65, 514-23. DOI
120. Cao, J.; Wang, Y.; Chen, Y.; et al. Improved sodium storage properties of co-doped $\text{Na}_3\text{V}_2(\text{PO}_4)_2\text{F}_3$ @graphene as anode material for sodium ion batteries. *Ferroelectrics* **2021**, 584, 221-9. DOI
121. Gu, Z. Y.; Guo, J. Z.; Sun, Z. H.; et al. Aliovalent-ion-induced lattice regulation based on charge balance theory: advanced fluorophosphate cathode for sodium-ion full batteries. *Small* **2021**, 17, e2102010. DOI
122. Zhang, Y.; Guo, S.; Xu, H. Synthesis of uniform hierarchical $\text{Na}_{3.195}\text{Mn}_{0.05}(\text{PO}_4)_2\text{F}_3$ @C hollow microspheres as a cathode material for sodium-ion batteries. *J. Mater. Chem. A*. **2018**, 6, 4525-34. DOI
123. Li, L.; Xu, Y.; Chang, R.; Wang, C.; He, S.; Ding, X. Unraveling the mechanism of optimal concentration for Fe substitution in $\text{Na}_3\text{V}_2(\text{PO}_4)_2\text{F}_3$ /C for sodium-ion batteries. *Energy. Storage. Mater.* **2021**, 37, 325-35. DOI
124. Gu, Z.; Guo, J.; Zhao, X.; et al. High-ionicity fluorophosphate lattice via aliovalent substitution as advanced cathode materials in sodium-ion batteries. *InfoMat* **2021**, 3, 694-704. DOI
125. Missaoui, K.; Ferchichi, K.; Amdouni, N.; et al. Polyaniline-coated $\text{Na}_3\text{V}_2(\text{PO}_4)_2\text{F}_3$ cathode enables fast sodium ion diffusion and structural stability in rechargeable batteries. *ACS. Appl. Mater. Interfaces.* **2024**, 16, 50550-60. DOI
126. Mani, K. P. L.; Venkatesh, M.; Nandy, S.; et al. Outstanding specific energy achieved via reversible cycling of $\text{V}^{4+}/\text{V}^{2+}$ redox couple in N-doped carbon coated $\text{Na}_3\text{V}_2(\text{PO}_4)_2\text{F}_3$: an *ex-situ* XRD, XPS and XAS study. *Mater. Today. Energy.* **2025**, 48, 101802. DOI
127. Sun, C.; Zhang, L.; Deng, Z.; Yan, B.; Gao, L.; Yang, X. PTFE-derived carbon-coated $\text{Na}_3\text{V}_2(\text{PO}_4)_2\text{F}_3$ cathode material for high-performance sodium ion battery. *Electrochimica. Acta.* **2022**, 432, 141187. DOI
128. Hu, Y.; Chen, P.; Liu, F.; et al. Dual-anion ether electrolyte enables stable high-voltage $\text{Na}_3\text{V}_2(\text{PO}_4)_2\text{F}_3$ cathode under wide temperatures. *J. Power. Sources.* **2024**, 602, 234405. DOI
129. Zhao, W.; Wang, W.; Hu, G.; et al. Facial construction of high rate $\text{Na}_3\text{V}_2(\text{PO}_4)_2\text{F}_3$ /C microspheres with fluorocarbon layer by deep-eutectic solvent synthesis. *Electrochimica. Acta.* **2023**, 440, 141718. DOI
130. Yang, X.; Wang, M.; Xiang, X.; Liu, S.; Chen, C. An open-system synthesis approach to achieve high-rate $\text{Na}_3(\text{VO})_2(\text{PO}_4)_2\text{F}$ /C microcubes cathode for sodium-ion batteries. *J. Electroanal. Chem.* **2024**, 956, 118088. DOI
131. Zhang, Y.; Song, W.; Tang, Y.; Jia, D.; Huang, Y. Amylopectin-assisted fabrication of *in situ* carbon-coated $\text{Na}_3\text{V}_2(\text{PO}_4)_2\text{F}_3$ nanosheets for ultra-fast sodium storage. *ACS. Appl. Mater. Interfaces.* **2022**, 14, 40812-21. DOI
132. Wang, M.; Wang, Y.; Xin, Y.; Liu, Q.; Wu, F.; Gao, H. Nitrogen-doped carbon coated $\text{Na}_3\text{V}_2(\text{PO}_4)_2\text{F}_3$ derived from polyvinylpyrrolidone as a high-performance cathode for sodium-ion batteries. *ACS. Appl. Energy. Mater.* **2023**, 6, 4453-61. DOI
133. Sun, C.; Zhang, L. L.; Deng, Z. R.; Sun, H. B.; Yang, X. L. Achieving high-performance $\text{Na}_3\text{V}_2(\text{PO}_4)_2\text{F}_3$ cathode material through a

- bifunctional N-doped carbon network. *ACS. Appl. Mater. Interfaces*. **2024**, *16*, 35179-89. DOI PubMed
134. Xu, J.; Tang, A.; Wen, Q.; et al. N/S dual-doped KB-decorated $\text{Na}_3\text{V}_2(\text{PO}_4)_2\text{F}_3$ as high-performance cathode for advanced sodium storage properties. *Ionics* **2024**, *30*, 7037-49. DOI
135. Wang, A.; Tian, Z.; Li, X.; Chai, Y.; Wang, N. Codoping of carbon and boron composition in $\text{Na}_3\text{V}_2(\text{PO}_4)_2\text{F}_3$ affects its sodium storage properties. *J. Electroanal. Chem.* **2024**, *974*, 118741. DOI
136. Zhang, X.; Tian, H.; Zhang, Y.; Cai, Y.; Yao, X.; Su, Z. Diatomic-doped carbon layer decorated $\text{Na}_3\text{V}_2(\text{PO}_4)_2\text{F}_3$ as a durable ultrahigh-stability cathode for sodium ion batteries. *New. J. Chem.* **2023**, *47*, 9611-7. DOI
137. Yu, X.; Lu, T.; Li, X.; et al. Realizing outstanding electrochemical performance with $\text{Na}_3\text{V}_2(\text{PO}_4)_2\text{F}_3$ modified with an ionic liquid for sodium-ion batteries. *RSC. Adv.* **2022**, *12*, 14007-17. DOI PubMed PMC
138. Yu, X.; Lu, T.; Li, X.; et al. Ionic liquid-acrylic acid copolymer derived nitrogen-boron codoped carbon-covered $\text{Na}_3\text{V}_2(\text{PO}_4)_2\text{F}_3$ as cathode material of high-performance sodium-ion batteries. *Langmuir* **2022**, *38*, 7815-24. DOI
139. Zhang, X.; Tian, H.; Cai, Y.; Wang, L.; Yao, X.; Su, Z. Effects of nitrogen and sulfur atom regulation on electrochemical properties of $\text{Na}_3\text{V}_2(\text{PO}_4)_2\text{F}_3$ cathode material for Na-ion batteries. *Ceram. Int.* **2022**, *48*, 36129-35. DOI
140. Tang, K.; Tian, H.; Zhang, Y.; et al. Multilevel carbon composite construction of NASICON-type $\text{NaVPO}_4\text{F/C/CNT}$ cathode material for enhanced-performance sodium-ion batteries. *J. Mater. Chem. C*. **2025**, *13*, 6605-13. DOI
141. Ma, W. L.; Zhou, Y.; Zhao, X. W.; et al. Ultra-fast-charging, long-duration, and wide-temperature-range sodium storage enabled by multiwalled carbon nanotube-hybridized biphasic polyanion-type phosphate cathode materials. *ACS. Appl. Mater. Interfaces*. **2024**, *16*, 34819-29. DOI
142. Li, L.; Qin, Y.; Zhang, S.; et al. Ion transport through carbon nanotubes enable highly crystalline $\text{Na}_3\text{V}_2(\text{PO}_4)_2\text{F}_3$ cathode for ultra-stable sodium-ion storage. *J. Power. Sources*. **2023**, *576*, 233226. DOI
143. Zhang, Q.; Sun, X.; Liu, K.; Xu, Q.; Zheng, S.; Dai, S. Synergistic coupling effect of electronic conductivity and interphase compatibility on high-voltage $\text{Na}_3\text{V}_2(\text{PO}_4)_2\text{F}_3$ cathodes. *ACS. Sustainable. Chem. Eng.* **2023**, *11*, 12992-3001. DOI
144. Gao, J.; Tian, Y.; Ni, L.; et al. Robust cross-linked $\text{Na}_3\text{V}_2(\text{PO}_4)_2\text{F}_3$ full sodium-ion batteries. *Energy. Environ. Mater.* **2024**, *7*, e12485. DOI
145. Qin, M.; Qin, N.; Lei, M.; et al. Construction of $\text{Na}_3\text{V}_2(\text{PO}_4)_2\text{F}_3\text{/C/CNTs}$ nanocomposites with three-dimensional conductive network as cathode materials for sodium-ion batteries. *J. Electroanal. Chem.* **2022**, *920*, 116613. DOI
146. He, J.; Tao, T.; Yang, F.; Sun, Z.; Huang, H. Phase-manipulated hierarchically core-shell $\text{Na}_3(\text{VO}_{1-x}\text{PO}_4)_2\text{F}_{1+2x}$ ($0 \leq x \leq 1$)@ $\text{Na}_3\text{V}_2(\text{PO}_4)_3$ and its synergistic effect with conformally wrapped reduced graphene oxide framework towards high-performance cathode for sodium-ion batteries. *Mater. Today. Phys.* **2022**, *27*, 100813. DOI
147. Xu, S.; Zhu, Y.; Li, X.; et al. PVA-regulated construction of 3D rGO-hosted $\text{Na}_3\text{V}_2(\text{PO}_4)_2\text{F}_3$ for fast and stable sodium storage. *J. Energy. Chem.* **2024**, *99*, 100-9. DOI
148. Huang, Q.; Shao, L.; Shi, X.; et al. $\text{Na}_3\text{V}_2\text{O}_2(\text{PO}_4)_2\text{F}$ nanoparticles@reduced graphene oxide: a high-voltage polyanionic cathode with enhanced reaction kinetics for aqueous zinc-ion batteries. *Chem. Eng. J.* **2023**, *468*, 143738. DOI
149. Ou, J.; Wang, H.; Deng, H.; Li, B.; Zhang, H. Hydrothermally prepared composite of $\text{Na}_3\text{V}_2(\text{PO}_4)_2\text{F}_3$ with gelatin and graphene used as a high-performance sodium ion battery cathode. *J. Alloys. Compd.* **2022**, *926*, 166857. DOI
150. Shi, C.; Xu, J.; Tao, T.; et al. Zero-Strain $\text{Na}_3\text{V}_2(\text{PO}_4)_2\text{F}_3\text{/Rgo/CNT}$ composite as a wide-temperature-tolerance cathode for Na-ion batteries with ultrahigh-rate performance. *Small. Methods*. **2024**, *8*, e2301277. DOI
151. Zheng, Q.; Ni, X.; Lin, L.; et al. Towards enhanced sodium storage by investigation of the Li ion doping and rearrangement mechanism in $\text{Na}_3\text{V}_2(\text{PO}_4)_2\text{F}_3$ for sodium ion batteries. *J. Mater. Chem. A*. **2018**, *6*, 4209-18. DOI
152. Kuang, Q.; Zhao, Y.; Liang, Z. Synthesis and electrochemical properties of Na-doped $\text{Li}_3\text{V}_2(\text{PO}_4)_3$ cathode materials for Li-ion batteries. *J. Power. Sources*. **2011**, *196*, 10169-75. DOI
153. Wu, Q.; Ma, Y.; Zhang, S.; et al. Achieving a rapid Na^+ migration and highly reversible phase transition of NASICON for sodium-ion batteries with suppressed voltage hysteresis and ultralong lifespan. *Small* **2024**, *20*, e2404660. DOI
154. Fu, W.; Li, B.; Wang, P.; Lin, Z.; Zhu, K. A high-entropy carbon-coated $\text{Na}_3\text{V}_{1.9}(\text{Mg, Cr, Al, Mo, Nb})_{0.1}(\text{PO}_4)_2\text{F}_3$ cathode for superior performance sodium-ion batteries. *Ceram. Int.* **2024**, *50*, 16166-71. DOI
155. Yang, J.; Liu, N.; Jiang, G.; et al. Synthesis and investigation of sodium storage properties in $\text{Na}_3\text{V}_{1.9}\text{Fe}_{0.1}(\text{PO}_4)_2\text{F}_3\text{/N-CNTs}$ cathode material for sodium ion batteries. *Chem. Eng. J.* **2024**, *485*, 149834. DOI
156. Puspitasari, D. A.; Patra, J.; Hung, I.; Bresser, D.; Lee, T.; Chang, J. Optimizing the Mg doping concentration of $\text{Na}_3\text{V}_{2-x}\text{Mg}_x(\text{PO}_4)_2\text{F}_3\text{/C}$ for enhanced sodiation/desodiation properties. *ACS. Sustainable. Chem. Eng.* **2021**, *9*, 6962-71. DOI
157. Ren, K.; Qiu, J.; Liu, H.; Song, H.; Li, Q.; Li, J. Low-valence Mg^{2+} doping suppresses irreversible phase transition of sodium-rich fluorophosphate upon additional Na^+ deintercalation. *ACS. Appl. Energy. Mater.* **2025**, *8*, 3066-73. DOI
158. Olchowka, J.; Nguyen, L. H. B.; Broux, T.; et al. Aluminum substitution for vanadium in the $\text{Na}_3\text{V}_2(\text{PO}_4)_2\text{F}_3$ and $\text{Na}_3\text{V}_2(\text{PO}_4)_2\text{FO}_2$ type materials. *Chem. Commun. (Camb)*. **2019**, *55*, 11719-22. DOI PubMed
159. Pineda-Aguilar, N.; Gallegos-Sánchez, V. J.; Sánchez, E. M.; Torres-gonzález, L. C.; Garza-tovar, L. L. Aluminum doped $\text{Na}_3\text{V}_2(\text{PO}_4)_2\text{F}_3$ via sol-gel Pechini method as a cathode material for lithium ion batteries. *J. Sol-Gel. Sci. Technol.* **2017**, *83*, 405-12. DOI
160. Wang, J.; Liu, Q.; Cao, S.; Zhu, H.; Wang, Y. Boosting sodium-ion battery performance with binary metal-doped $\text{Na}_3\text{V}_2(\text{PO}_4)_2\text{F}_3$ cathodes. *J. Colloid. Interface. Sci.* **2024**, *665*, 1043-53. DOI
161. Chen, Q.; Gong, F.; Pan, S.; Chen, W. Effects of Bi doping on the electrochemical performance of $\text{Na}_3\text{V}_2(\text{PO}_4)_3\text{F}_3$ cathode material

- for sodium ion batteries. *Solid. State. Ionics.* **2024**, 414, 116621. DOI
162. Puspitasari, D. A.; Patra, J.; Hernandha, R. F. H.; et al. Enhanced electrochemical performance of Ca-doped $\text{Na}_3\text{V}_2(\text{PO}_4)_2\text{F}_3/\text{C}$ cathode materials for sodium-ion batteries. *ACS. Appl. Mater. Interfaces.* **2024**, 16, 496-506. DOI
 163. Silva, C. H. P.; de, O. L. J. L.; Rezende, M. V. D. S. Intrinsic defect and deformation on local structure caused by rare-earth ions in the $\text{Na}_3\text{V}_2(\text{PO}_4)_2\text{F}_3$ cathode material. *Physica. Status. Solidi. (b).* **2024**, 261, 2300348. DOI
 164. Ghosh, S.; Barman, N.; Mazumder, M.; Pati, S. K.; Rousse, G.; Senguttuvan, P. High capacity and high-rate NASICON- $\text{Na}_{3.75}\text{V}_{1.25}\text{Mn}_{0.75}(\text{PO}_4)_3$ cathode for Na-ion batteries via modulating electronic and crystal structures. *Adv. Energy. Mater.* **2020**, 10, 1902918. DOI
 165. Li, T.; Yang, D.; Xu, G.; et al. A novel NASICON-typed $\text{Na}_3\text{V}_{1.96}\text{Cr}_{0.03}\text{Mn}_{0.01}(\text{PO}_4)_2\text{F}_3$ cathode for high-performance Na-ion batteries. *J. Energy. Storage.* **2024**, 104, 114596. DOI
 166. Cai, C.; Liu, Q.; Hu, Z.; et al. Construction of superior performance $\text{Na}_3\text{V}_{2-x}\text{Cr}_x(\text{PO}_4)_2\text{F}_3/\text{C}$ cathode by homovalent doping strategy toward enhanced sodium ion storage. *J. Power. Sources.* **2023**, 571, 233080. DOI
 167. Yi, X.; Luo, H.; Zhou, Y.; et al. Effect of Cr^{3+} doping on the electrochemical performance of $\text{Na}_3\text{V}_2(\text{PO}_4)_2\text{F}_3/\text{C}$ cathode materials for sodium ion battery. *Electrochimica. Acta.* **2023**, 437, 141491. DOI
 168. Gu, Z.; Heng, Y.; Guo, J.; et al. Nano self-assembly of fluorophosphate cathode induced by surface energy evolution towards high-rate and stable sodium-ion batteries. *Nano. Res.* **2023**, 16, 439-48. DOI
 169. Su, R.; Zhu, W.; Liang, K.; et al. Mn^{x+} substitution to improve $\text{Na}_3\text{V}_2(\text{PO}_4)_2\text{F}_3$ -based electrodes for sodium-ion battery cathode. *Molecules* **2023**, 28, 1409. DOI PubMed PMC
 170. Tong, S.; Pan, H.; Liu, H.; et al. Titanium doping induced the suppression of irreversible phase transformation at high voltage for V-based phosphate cathodes of Na-ion batteries. *ChemSusChem* **2023**, 16, e202300244. DOI
 171. Nongkynrih, J.; Sengupta, A.; Modak, B.; Mitra, S.; Tyagi, A.; Dutta, D. P. Enhanced electrochemical properties of W-doped $\text{Na}_3\text{V}_2(\text{PO}_4)_2\text{F}_3/\text{C}$ as cathode material in sodium ion batteries. *Electrochimica. Acta.* **2022**, 415, 140256. DOI
 172. Zhu, L.; Zhang, Q.; Sun, D.; et al. Engineering the crystal orientation of $\text{Na}_3\text{V}_2(\text{PO}_4)_2\text{F}_3/\text{rGO}$ microcuboids for advanced sodium-ion batteries. *Mater. Chem. Front.* **2020**, 4, 2932-42. DOI
 173. Park, S.; Song, J.; Kim, S.; et al. Phase-pure $\text{Na}_3\text{V}_2(\text{PO}_4)_2\text{F}_3$ embedded in carbon matrix through a facile polyol synthesis as a potential cathode for high performance sodium-ion batteries. *Nano. Res.* **2019**, 12, 911-7. DOI
 174. Liu, S.; Cao, X.; Zhang, Y.; et al. Carbon quantum dot modified $\text{Na}_3\text{V}_2(\text{PO}_4)_2\text{F}_3$ as a high-performance cathode material for sodium-ion batteries. *J. Mater. Chem. A.* **2020**, 8, 18872-9. DOI
 175. Ponrouch, A.; Dedryvère, R.; Monti, D.; et al. Towards high energy density sodium ion batteries through electrolyte optimization. *Energy. Environ. Sci.* **2013**, 6, 2361. DOI
 176. Sadan, M. K.; Kim, H.; Kim, C.; et al. Enhanced rate and cyclability of a porous $\text{Na}_3\text{V}_2(\text{PO}_4)_3$ cathode using dimethyl ether as the electrolyte for application in sodium-ion batteries. *J. Mater. Chem. A.* **2020**, 8, 9843-9. DOI
 177. Hwang, J.; Matsumoto, K.; Hagiwara, R. Electrolytes toward high-voltage $\text{Na}_3\text{V}_2(\text{PO}_4)_2\text{F}_3$ positive electrode durable against temperature variation. *Adv. Energy. Mater.* **2020**, 10, 2001880. DOI
 178. Liu, F.; Zong, J.; Liang, Y.; et al. Ordered vacancies as sodium ion micropumps in Cu-deficient copper indium diselenide to enhance sodium storage. *Adv. Mater.* **2024**, 36, e2403131. DOI
 179. Li, J.; Liang, Z.; Jin, Y.; et al. A high-voltage cathode material with ultralong cycle performance for sodium-ion batteries. *Small. Methods.* **2024**, 8, e2301742. DOI
 180. Xie, K.; Ji, Y.; Yang, L.; Pan, F. Electrolyte design strategies to construct stable cathode-electrolyte interphases for high-voltage sodium-ion batteries. *Adv. Energy. Mater.* **2025**, 15, 2405301. DOI
 181. Alptekin, H.; Au, H.; Olsson, E.; et al. Elucidation of the solid electrolyte interphase formation mechanism in micro-mesoporous hard-carbon anodes. *Adv. Mater. Inter.* **2022**, 9, 2101267. DOI
 182. Zhang, J.; Li, J.; Jia, G.; Wang, H.; Wang, M. Improving $\text{Na}_3\text{V}_2(\text{PO}_4)_2\text{F}_3$ half-cell performance with NaBF_4 -enhanced sodium difluoro(oxalato)borate electrolyte. *J. Energy. Chem.* **2025**, 102, 340-52. DOI
 183. Liang, H.; Liu, H.; Guo, J.; et al. Self-purification and silicon-rich interphase achieves high-temperature (70 °C) sodium-ion batteries with nonflammable electrolyte. *Energy. Storage. Mater.* **2024**, 66, 103230. DOI
 184. Liang, H. J.; Liu, H. H.; Zhao, X. X.; et al. Electrolyte chemistry toward ultrawide-temperature (-25 to 75 °C) sodium-ion batteries achieved by phosphorus/silicon-synergistic interphase manipulation. *J. Am. Chem. Soc.* **2024**, 146, 7295-304. DOI
 185. Ren, H.; Zhang, X.; Liu, Q.; Tang, W.; Liang, J.; Wu, W. Fully-printed flexible aqueous rechargeable sodium-ion batteries. *Small* **2024**, 20, e2312207. DOI
 186. Desai, P.; Forero-Saboya, J.; Meunier, V.; et al. Mastering the synergy between $\text{Na}_3\text{V}_2(\text{PO}_4)_2\text{F}_3$ electrode and electrolyte: a must for Na-ion cells. *Energy. Storage. Mater.* **2023**, 57, 102-17. DOI
 187. Zheng, Y.; Sun, M.; Yu, F.; et al. Utilizing weakly-solvated diglyme-based electrolyte to achieve a 10,000-cycles durable $\text{Na}_3\text{V}_2(\text{PO}_4)_2\text{F}_3$ cathode endured at -20 °C. *Nano. Energy.* **2022**, 102, 107693. DOI
 188. Wang, X.; Yang, C.; Yao, L.; Wang, Y.; Jiang, N.; Liu, Y. Anion/Cation solvation engineering for a ternary low-concentration electrolyte toward high-voltage and long-life sodium-ion batteries. *Adv. Funct. Mater.* **2024**, 34, 2315007. DOI
 189. Jiang, M.; Li, T.; Qiu, Y.; et al. Electrolyte design with dual $\text{C}\equiv\text{N}$ groups containing additives to enable high-voltage $\text{Na}_3\text{V}_2(\text{PO}_4)_2\text{F}_3$ -based sodium-ion batteries. *J. Am. Chem. Soc.* **2024**, 146, 12519-29. DOI
 190. Hwang, J.; Aoyagi, I.; Takiyama, M.; Matsumoto, K.; Hagiwara, R. Inhibition of aluminum corrosion with the addition of the

- tris(pentafluoroethyl)trifluorophosphate anion to a sulfonylamide-based ionic liquid for sodium-ion batteries. *J. Electrochem. Soc.* **2022**, *169*, 080522. DOI
191. Yan, Y.; Xu, J.; Cao, J.; et al. Fluorinated ionic liquid mediated nanostructure with enhanced conductivity and fluorine retention in $\text{Na}_3\text{V}_2(\text{PO}_4)_2\text{F}_3$ cathode toward high-performance sodium-ion batteries. *Chem. Eng. J.* **2024**, *498*, 155640. DOI
192. Li, Z.; Qiu, L.; Li, P.; et al. Exposing the (002) active facet by reducing surface energy for a high-performance $\text{Na}_3\text{V}_2(\text{PO}_4)_2\text{F}_3$ cathode. *J. Mater. Chem. A*. **2024**, *12*, 7777-87. DOI
193. Zhang, S.; Wang, J.; Chen, K.; et al. Aromatic ketones as mild presodiating reagents toward cathodes for high-performance sodium-ion batteries. *Angew. Chem. Int. Ed. Engl.* **2024**, *63*, e202317439. DOI
194. Yun, D. H.; Song, J.; Kim, J.; et al. A binder-driven cathode-electrolyte interphase via a displacement reaction for high voltage $\text{Na}_3\text{V}_2(\text{PO}_4)_2\text{F}_3$ cathodes in sodium-ion batteries. *J. Mater. Chem. A*. **2023**, *11*, 5540-7. DOI
195. Zhang, Z.; Zhang, R.; Rajagopalan, R.; et al. A high-capacity self-sacrificial additive based on electroactive sodiated carbonyl groups for sodium-ion batteries. *Chem. Commun. (Camb)*. **2022**, *58*, 8702-5. DOI
196. Forero-saboya, J.; Desai, P.; Healy, C. R.; et al. Influence of formation temperature on cycling stability of sodium-ion cells: a case study of $\text{Na}_3\text{V}_2(\text{PO}_4)_2\text{F}_3/\text{HC}$ Cells. *J. Electrochem. Soc.* **2023**, *170*, 100529. DOI
197. Komayko, A. I.; Shraer, S. D.; Fedotov, S. S.; Nikitina, V. A. Advantages of a solid solution over biphasic intercalation for vanadium-based polyanion cathodes in Na-ion batteries. *ACS. Appl. Mater. Interfaces*. **2023**, *15*, 43767-77. DOI PubMed
198. Goloviznina, K.; Bendadesse, E.; Sel, O.; Tarascon, J. M.; Salanne, M. Disclosing the interfacial electrolyte structure of Na-insertion electrode materials: origins of the desolvation phenomenon. *ACS. Appl. Mater. Interfaces*. **2023**, *15*, 59380-8. DOI PubMed
199. Semykina, D. O.; Sharafutdinov, M. R.; Kosova, N. V. Understanding of the mechanism and kinetics of the fast solid-state reaction between NaF and VPO_4 to form $\text{Na}_3\text{V}_2(\text{PO}_4)_2\text{F}_3$. *Inorg. Chem.* **2022**, *61*, 10023-35. DOI
200. Deng, L.; Yu, F. D.; Sun, G.; et al. Constructing stable anion-tuned electrode/electrolyte interphase on high-voltage $\text{Na}_3\text{V}_2(\text{PO}_4)_2\text{F}_3$ cathode for thermally-modulated fast-charging batteries. *Angew. Chem. Int. Ed. Engl.* **2022**, *61*, e202213416. DOI
201. Zhang, Y.; Xun, J.; Zhang, K.; Zhang, B.; Xu, H. 2D-lamellar stacked $\text{Na}_3\text{V}_2(\text{PO}_4)_2\text{F}_3/\text{RuO}_2$ as a high-voltage, high-rate capability and long-term cycling cathode material for sodium ion batteries. *J. Mater. Chem. A*. **2022**, *10*, 11163-71. DOI
202. S., Biswas, K. Boosting sodium-ion battery performance with vanadium substituted Fe, Ni dual doped fluorophosphate cathode over a wide temperature range. *J. Power. Sources*. **2025**, *626*, 235734. DOI